

# 1 Assembly of 43 diverse human Y chromosomes reveals 2 extensive complexity and variation

3  
4 Pille Hallast<sup>1,\*</sup>, Peter Ebert<sup>2,3,\*</sup>, Mark Loftus<sup>4</sup>, Feyza Yilmaz<sup>1</sup>, Peter A. Audano<sup>1</sup>, Glennis A. Logsdon<sup>5</sup>,  
5 Marc Jan Bonder<sup>6</sup>, Weichen Zhou<sup>7</sup>, Wolfram Höps<sup>8</sup>, Kwondo Kim<sup>1</sup>, Chong Li<sup>9</sup>, Philip Dishuck<sup>5</sup>, David  
6 Porubsky<sup>5</sup>, Fotios Tsetsos<sup>1</sup>, Jee Young Kwon<sup>1</sup>, Qihui Zhu<sup>1</sup>, Katherine M. Munson<sup>5</sup>, Patrick Hasenfeld<sup>8</sup>,  
7 William T. Harvey<sup>5</sup>, Alexandra P. Lewis<sup>5</sup>, Jennifer Kordosky<sup>5</sup>, Kendra Hoekzema<sup>5</sup>, The Human  
8 Genome Structural Variation Consortium (HGSVC), Jan O. Korbel<sup>8</sup>, Chris Tyler-Smith<sup>10</sup>, Evan E.  
9 Eichler<sup>5,11</sup>, Xinghua Shi<sup>9</sup>, Christine R. Beck<sup>1,12</sup>, Tobias Marschall<sup>2</sup>, Miriam K. Konkel<sup>4</sup>, Charles Lee<sup>1</sup>

10

11 <sup>1</sup>The Jackson Laboratory for Genomic Medicine, Farmington, CT, USA

12 <sup>2</sup>Institute for Medical Biometry and Bioinformatics, Medical Faculty, Heinrich Heine University,  
13 Düsseldorf, Germany

14 <sup>3</sup>Core Unit Bioinformatics, Medical Faculty, Heinrich Heine University, Düsseldorf, Germany

15 <sup>4</sup>Clemson University, Department of Genetics & Biochemistry, Clemson, SC, USA

16 <sup>5</sup>University of Washington School of Medicine, Department of Genome Sciences, Seattle, WA, USA

17 <sup>6</sup>German Cancer Research Center (DKFZ), Division of Computational Genomics and Systems  
18 Genetics, Heidelberg, Germany

19 <sup>7</sup>University of Michigan Medical School, Department of Computational Medicine and Bioinformatics,  
20 Ann Arbor, MI, USA

21 <sup>8</sup>European Molecular Biology Laboratory (EMBL), Genome Biology Unit, Heidelberg, Germany

22 <sup>9</sup>Temple University, Department of Computer and Information Sciences, Philadelphia, PA, USA

23 <sup>10</sup>Wellcome Sanger Institute, Wellcome Genome Campus, Hinxton, UK

24 <sup>11</sup>Howard Hughes Medical Institute, University of Washington, Seattle, WA, USA

25 <sup>12</sup>The University of Connecticut Health Center, Farmington, CT, USA

26

27 \*These authors contributed equally to this work

28 Correspondence to: Charles Lee [charles.lee@jax.org](mailto:charles.lee@jax.org)

29

## 30 Abstract

31 The prevalence of highly repetitive sequences within the human Y chromosome has led to its incomplete  
32 assembly and systematic omission from genomic analyses. Here, we present long-read *de novo*  
33 assemblies of 43 diverse Y-chromosomes, three contiguously assembled including two from deep-  
34 rooted African Y lineages. Examination of the full extent of genetic variation between Y chromosomes  
35 across 180,000 years of human evolution reveals its remarkable complexity and diversity in size and  
36 structure, in contrast with its low level of base substitution variation. The size of the Y chromosome  
37 assemblies vary extensively from 45.2 to 84.9 Mbp, with individual repeat arrays showing up to 6.7-  
38 fold difference in length across samples. Half of the male-specific euchromatic region is subject to large  
39 (up to 5.94 Mbp) inversions with a >2-fold higher recurrence rate compared to the rest of the human  
40 genome. The Y centromere, composed of 171 bp  $\alpha$ -satellite monomer units, appears to have evolved  
41 from tandem arrays of a 36-mer ancestral higher order repeat (HOR), which has been predominantly  
42 replaced by a 34-mer HOR, and reveals a pattern of higher sequence variation towards the short-arm  
43 side. The Yq12 heterochromatic region is ubiquitously flanked by approximately 649 kbp and 472 kbp  
44 inversions that maintain the alternating arrays of *DYZ1* and *DYZ2* repeat units in between. While the  
45 sizes and the distribution of the *DYZ1* and *DYZ2* arrays vary considerably, primarily due to local  
46 expansions and contractions, the copy number ratio between the *DYZ1* and *DYZ2* monomer repeat units  
47 remains consistently close to 1:1. In addition, we have identified on average 65 kbp of novel sequence  
48 per Y chromosome. The availability of sequence-resolved Y chromosomes from multiple samples  
49 provides a basis for identifying new associations of specific traits with the Y chromosome and garnering  
50 novel evolutionary insights.

51

## 52 Introduction

53 The mammalian sex chromosomes evolved from a pair of autosomes, gradually losing their  
54 ability to recombine over increasing lengths, leading to degradation and accumulation of large  
55 proportions of repetitive sequences<sup>1</sup>. The resulting sequence composition of the human Y chromosome  
56 is rich in complex repetitive regions, including highly similar segmental duplications (SDs)<sup>2,3</sup>. This has  
57 made the Y chromosome difficult to assemble, and, paired with reduced gene content, has led to its  
58 systematic neglect in genomic analyses.

59 The first human Y chromosome sequence assembly was generated almost 20 years ago via a  
60 laborious approach of mapping and Sanger sequencing of bacterial artificial chromosome (BAC)  
61 clones, which provided a high quality but incomplete sequence (~30.8/57.2 Mbp unresolved in  
62 GRCh38)<sup>3</sup>. Less than half (~25 Mbp) of the GRCh38 Y chromosome is composed of euchromatin which  
63 contains two pseudoautosomal regions, PAR1 and PAR2 (~3.2 Mbp in total), that actively recombine  
64 with homologous regions on the X chromosome and are therefore not considered as part of the male-  
65 specific Y region (MSY)<sup>3</sup>. The remainder of the Y-chromosomal euchromatin (~22 Mbp) has been  
66 divided into three main classes according to their sequence composition and evolutionary history<sup>3</sup>: (i)  
67 the X-degenerate regions (XDR, ~8.6 Mbp) are remnants of the ancient autosomes from which the X  
68 and Y chromosomes evolved, (ii) the X-transposed regions (XTR, ~3.4 Mbp) resulted from a  
69 duplicative transposition event from the X chromosome followed by an inversion, and (iii) the  
70 ampliconic regions (~9.9 Mbp) that contain sequences having up to 99.9% intra-chromosomal identity  
71 across tens or hundreds of kilobases (**Fig. 1a**). The rest of the Y chromosome is largely composed of  
72 repetitive centromeric and heterochromatic sequences, including the (peri-)centromeric *DYZ3*  $\alpha$ -  
73 satellite and *DYZ17* arrays, *DYZ18* and *DYZ19* arrays, and the large Yq12 block, which is known to be  
74 highly variable in size<sup>3,4,5</sup>. All these heterochromatic regions are thought to be predominantly satellites,  
75 simple repeats and segmental duplications<sup>3,6</sup>.

76 The current 57.2 Mbp GRCh38 Y reference assembly is a patched version of the 2003 Sanger  
77 assembly and is still structurally incomplete, as it is composed of 53.8% missing sequence (N's) (**Fig.**  
78 **1a**). Past attempts have been made to assemble the human Y chromosome using Illumina short-read<sup>7</sup>  
79 and Oxford Nanopore Technologies (ONT) long-read data<sup>8</sup>, but a contiguous assembly of the  
80 ampliconic and heterochromatic regions was not achieved.

81 In April 2022, the first complete *de novo* assembly of a human Y chromosome (from individual  
82 HG002/NA24385, carrying a rare J1a-L816 Y lineage found among Ashkenazi Jews and Europeans<sup>9</sup>),  
83 was deposited in GenBank by the Telomere-to-Telomere (T2T) Consortium<sup>10</sup>. However, understanding  
84 the composition and appreciating the complexity of the Y chromosomes in the human population  
85 requires access to assemblies from many diverse individuals. Here, we have combined PacBio HiFi and  
86 ONT long-read sequence data to assemble the Y chromosomes from 43 males, representing the five  
87 continental groups from the 1000 Genomes Project. While both the GRCh38 (mostly R1b-L20

88 haplogroup) and the T2T Y represent European Y lineages, 21/43 (49%) of our Y chromosomes  
89 represent African lineages and include most of the deepest-rooting human Y lineages. This newly  
90 assembled dataset of 43 Y chromosomes thus provides a more comprehensive view of genetic variation  
91 at the nucleotide level across over 180,000 years of human Y chromosome evolution.

## 92 Results

### 93 *Sample Selection*

94 We selected 43 genetically diverse males from the 1000 Genomes Project that had  
95 accompanying data recently generated by the Human Genome Structural Variation Consortium  
96 (HGSVC) (n=28)<sup>11</sup> and the Human Pangenome Reference Consortium (HPRC) (n=15)<sup>12</sup> (**Table S1**).  
97 These 43 males include three samples carrying the deepest-rooting African Y lineages present among  
98 the 1000 Genomes Project (HG01890, HG02666 and NA19384, which carry A0b-L1038, A1a-M31  
99 and B2b-M112, respectively)<sup>13</sup> (**Fig. 1b**). The time to the most recent common ancestor (TMRCA)  
100 among our 43 Y chromosomes and the Y assembly from HG002/NA24385 (J1a-L816 haplogroup,  
101 termed as T2T Y) was estimated to be approximately 183 thousand years ago (kya) (95% HPD interval:  
102 160-209 kya) (**Fig. S1; Methods**), consistent with previous reports<sup>14,15</sup>. Additionally, a pair of closely-  
103 related African Y chromosomes, representing the E1b1a1a1a-CTS8030 lineage (NA19317 and  
104 NA19347), were included for assembly validation, as these Y chromosomes are expected to be highly  
105 similar (TMRCA 200 ya [95% HPD interval: 0 - 500 ya]). Taken together, the 43 samples we analyzed  
106 represent 21 largely African (haplogroups A, B and E)<sup>16</sup> and 22 non-African Y haplogroups (**Table S1**).  
107 Notably, there is an African Y lineage (A00) older than the lineages in our dataset (TMRCA 254 kya;  
108 95% CI 192-307 kya<sup>14,17</sup>) that we could not include due to sample availability issues. Nevertheless, our  
109 diverse samples cover genetic variation across a substantial period of modern human evolution (**Fig.**  
110 **1b,d; Fig. S1**).

111

### 112 *Constructing De Novo Assemblies*

113 We employed the hybrid assembler Verkko<sup>18</sup> to generate Y chromosome assemblies including  
114 the ampliconic and heterochromatic regions (**Methods**). Verkko leverages the high accuracy of PacBio  
115 HiFi reads (99.5% base pair calling accuracy) with the length of Oxford Nanopore Long/Ultra Long  
116 Reads (median read length N50 134 kbp) to produce highly accurate and contiguous assemblies (**Table**  
117 **S2**). Using this approach, we generated high-quality (median QV 48; **Table S3**) whole-genome (median  
118 length 5.9 Gbp; **Table S4**) assemblies for 43 male samples. The chromosome Y sequences exhibit a  
119 high degree of completeness (median length 55.6 Mbp, 79% to 148% assembly length relative to  
120 GRCh38 Y; **Fig. 1; Fig. S2; Table S5**), contiguity (median NG50 9.6 Mbp, median LG50 2) and base-  
121 pair quality (median QV 46, **Table S3**). The Verkko assembly process was robust (sequence identity  
122 for NA19317/NA19347 pair of 99.9959%, **Fig. S3; Table S6; Supplementary Results 'De novo**

123 **assembly evaluation**) and generated the complete Y chromosome assembly, spanning from PAR1 to  
124 PAR2, for three individuals (HG01890 haplogroup A0b-L1038, HG02666 haplogroup A1a-M31,  
125 HG00358 haplogroup N1c-Z1940; **Figs. 1b, 2; Table S7**). This study presents the first dataset where  
126 deep-rooting African Y chromosomes have been contiguously assembled to high quality. These three  
127 samples are among nine samples with an increased HiFi coverage of at least 50× (“high-coverage  
128 samples”, **Tables S1-S2**). The other six high-coverage samples were not completely assembled,  
129 indicating that increased HiFi coverage alone is not sufficient to ensure complete Y-chromosomal  
130 assembly (on average 2.5/24 Y-chromosomal subregions completely assembled, **Figs. 1c,e;**  
131 **Supplementary Results ‘Effect of input read characteristics on assembly contiguity’**).

132 Following established procedures<sup>11,19</sup>, we computed error rate estimates ranging from 0.04  
133 errors per kbp assembled Y sequence up to 7.6 errors per kbp (**Table S8; Methods**). The upper range  
134 of the annotated errors is dominated by a few outlier samples as indicated by a median and mean of  
135 0.77 and 1.28 ( $\pm 1.52$  s.d.) errors per kbp, respectively. Although the error rate is increased for the  
136 lower-coverage assemblies, increasing the HiFi coverage beyond 50× has limited effect on the error  
137 rate (**Figs. S4-S5**).

138 We further annotated each of the Y-chromosomal assemblies with respect to the 24 Y-  
139 chromosomal subregions originally proposed by Skaletsky and colleagues (**Fig. 1a-c; Fig. S2; Table**  
140 **S9; Methods**)<sup>3</sup> and looked in more detail at the assembly outcome of each of these subregions. In  
141 addition to the three complete Y chromosomes, we have contiguously assembled the MSY (excluding  
142 Yq12) for 10/43 samples and the MSY (excluding Yq12 and the (peri-)centromeric region) for 17/43  
143 samples (**Tables S7, S10-S11**). Overall, 17/24 subregions were contiguously assembled across 41/43  
144 samples (**Figs. 1b-c; Fig. S2**).

145

### 146 *Genomic and epigenetic variation of assembled Y chromosomes*

147 The assembled Y chromosomes showed extensive variation both in size and structure (**Figs.**  
148 **2a-c, 3a and 4; Figs. S6-S17; Methods**). The sizes of the Y assemblies ranged from 45.2 to 84.9 Mbp  
149 (mean 57.6 and median 55.7 Mbp, **Fig. S15; Table S5; Methods**), a 1.88-fold difference in size. The  
150 three complete Y chromosomes varied from 46.4 Mbp (our deepest-rooting A0b Y represented by  
151 HG01890) to 58.9 Mbp (HG00358; haplogroup N1c). In comparison, the T2T Y assembly from HG002  
152 (haplogroup J1a) is 62.5 Mbp in size, primarily due to expansion of the Yq12 heterochromatic  
153 subregion. In contrast, the MSY (excluding Yq12 subregion) for the 10 contiguously assembled  
154 individuals and the T2T Y varies by less than 2 Mbp (from 24.1 to 26.1 Mbp, mean 25.4 Mbp) (**Tables**  
155 **S10-S11**).

156 Among the contiguously assembled Y-chromosomal subregions the largest variation in size  
157 was seen in the heterochromatic Yq12 (17.6 to 37.2 Mbp, mean 27.6 Mbp), the (peri-)centromeric  
158 region (2.0 to 3.3 Mbp, mean 2.7 Mbp) and the *DYZ19* repeat array (63.5 to 428 kbp, mean 305.4 kbp)  
159 (**Figs. 2a, 4f; Figs. S15-S21; Tables S10-S11**). Phylogenetically, a relatively shorter size of the *DYZ19*

160 subregion was observed in ten samples representing the E1b1a1a haplogroup (from 217 to 247 kbp,  
161 mean 236 kbp), and an increased size (from 283 to 428 kbp, mean 369 kbp) among 17 phylogenetically-  
162 related haplogroup N, O, Q and R samples (**Figs. S17, S19-S22**).

163 The euchromatic regions show comparatively little variation in size (**Figs. 2a; Tables S10-**  
164 **S11**). The exception is the ampliconic subregion 2 which contains a highly copy-number variable repeat  
165 array, composed of approximately 20.3 kbp long repeat units and each containing a copy of the *TSPY*  
166 (testis specific protein Y-linked 1) gene (**Fig. 3c**), which accounts for up to 467 kbp size difference  
167 between samples (**Fig. S23; Tables S12-S13; Methods**). The *TSPY* repeat array was also found to be  
168 shorter in haplogroup QR samples (from 567 to 648 kbp, mean 603 kbp) compared to the rest of the  
169 samples (from 465 to 932 kbp, mean 701 kbp) (**Figs. S17, S23**). Such phylogenetic consistency offers  
170 support to the high quality of our assemblies even across homogeneous tandem arrays, as more closely  
171 related Y chromosomes are expected to be more similar, and consequently allows investigation of  
172 mutational dynamics across well-defined timeframes.

173 We produced a comprehensive set of variant calls using contig length to span across GRCh38  
174 euchromatin and heterochromatin (including 165 kbp of the Yq12 subregion present in GRCh38) and  
175 the fidelity of HiFi to resolve small variants and structural variants (SVs). In the MSY, we report on  
176 average 88 insertion and deletion structural variants (SVs,  $\geq 50$  bp), 3 large inversions ( $>1$  kbp), 2,168  
177 indels ( $< 50$  bp), and 3,228 single nucleotide variants (SNVs) (**Fig. S24; Table S14; Methods**). Variants  
178 were merged across all 43 samples to produce a nonredundant callset of 413 SVs, 10 inversions, 16,216  
179 indels, and 34,764 SNVs (**Tables S15-S19; Supplementary Results ‘Orthogonal support to Y-**  
180 **chromosomal SVs’**). The average SNV density on the MSY is 0.09 SNV / kbp, which is significantly  
181 less than any other chromosome including chromosome X and the Y-chromosomal PARs ( $p < 1.87 \times$   
182  $10^{-17}$ , Welch’s t-test). The next lowest density is chromosome X (0.73 SNV / kbp), and all other  
183 chromosomes including the Y-chromosomal PAR average 1.42 SNV / kbp (1.94 – 1.62 SNV / kbp)  
184 (**Table S20**). Based on insertion calls ( $\geq 50$  bp in size), we have identified from 30 to 140 kbp (mean  
185 65 kbp; or an average of 16 kbp after exclusion of mobile elements and simple repeats) of inserted  
186 sequences per Y chromosome that is not present in the GRCh38 Y reference sequence (**Table S21**).

187 While we identified no SVs that directly intersect known exons, a 47 kbp duplication in 15 of  
188 43 samples (35%) contains an additional copy of *RBMY1B*, a functional copy of RNA binding motif  
189 protein Y-linked family 1 (RBMY1). Duplicate copies contain two missense variants that do not appear  
190 to disrupt the gene. Previous studies have shown that fewer than six RBMY1 copies are associated with  
191 male infertility<sup>20</sup> and that low expression of *RBMY1B* in high-risk infertility cases can be upregulated  
192 by hormonal treatment with improved outcomes<sup>21</sup>. Taken together, this suggests that the observed  
193 *RBMY1B* duplication may be protective against male infertility. The results from variant calling overlap  
194 well with the gene annotation of the Y-chromosomal assemblies and showed that all protein-coding  
195 genes in the GRCh38 Y reference were present in the 43 Y chromosomes studied, except for 14 genes

196 in PAR1, 1 gene in XDR1 and 1 gene in PAR2 in a total of 14 individuals, overlapping with poorly  
197 assembled regions in those individuals (**Tables S22-S26; Supplementary Results ‘Gene annotation’**).

198 Additional large inversions were identified using Strand-seq and manual inspection of assembly  
199 alignments, which yielded a total of 14 inversions in the euchromatic regions of the Y chromosome and  
200 two inversions within the Yq12 subregion (**Figs. 3a, 4c; Figs. S25-S26; Tables S27-S28; Methods;  
201 Supplementary Results ‘Y-chromosomal Inversions’**). Seven of these matched the 10 inversions  
202 identified by variant calling. We have defined the breakpoint regions for 8/14 of the euchromatic  
203 inversions to DNA intervals as small as 500 bp (**Fig. 3b; Fig. S26-S28; Table S29; Methods**). All of  
204 these inversions are flanked by highly similar (up to 99.97%) and large (up to 1.45 Mbp) inverted  
205 segmental duplications, and while determination of the molecular mechanism generating Y-  
206 chromosomal inversions remains challenging, most are likely a result of non-allelic homologous  
207 recombination (NAHR). 12/14 (85%) of the euchromatic inversions are recurrent, occurring from 2 to  
208 13 times in the Y phylogeny and translate to an inversion rate estimate ranging from  $3.68 \times 10^{-5}$  (95%  
209 C.I.:  $3.25 - 4.17 \times 10^{-5}$ ) to  $2.39 \times 10^{-4}$  (95% C.I.:  $2.11 - 2.71 \times 10^{-4}$ ) per father-to-son Y transmission  
210 (**Table S27**), with the highest inversion recurrence seen among the 8 Y-chromosomal palindromes  
211 (called P1-P8, **Fig. 3a; Fig. S22**). Taken together, we calculate a rate of one recurrent inversion per 603  
212 (95% C.I.: 533 - 684) father-to-son Y transmissions. The per site per generation rate estimates for 12  
213 Y-chromosomal recurrent inversion are significantly higher (>2-fold difference between median  
214 estimates, two-tailed Mann-Whitney-Wilcoxon test,  $n=44$ ,  $p\text{-value}<0.0001$ ) than the rates previously  
215 estimated for 32 autosomal and X-chromosomal recurrent inversions<sup>22</sup>.

216 There are two fixed inversions on either side of the Yq12 subregion (**Fig. 4c; Fig. S29; Table  
217 S28; Supplementary Results ‘Y-chromosomal Inversions’**). The proximal inversion, which was  
218 observed in 10/11 individuals analyzed but completely deleted in HG01106, ranged from 358.9 to 820.7  
219 kbp in size (mean 649.0 kbp) (**Table S28**). The distal inversion, on other hand, was observed in all 11  
220 individuals and ranged from 259.5 to 641.4 kbp in size (mean 472.5 kbp). We resolved the exact  
221 breakpoints for these two inversions and found them to be identical among all individuals in which they  
222 were present. This suggests that the consistent presence of these two inversions at either end of the  
223 Yq12 subregion, may prevent unequal sister chromatid exchange from occurring, restricting expansion  
224 and contraction of the repeat units to the region between these two inversions.

225 We also identified 25 transposable elements in the 43 Y-chromosomal assemblies that are not  
226 present in the GRCh38 Y, including 18 *Alu* elements (4/18 within the Yq12 heterochromatic region)  
227 and 7 LINE-1 elements (no significant difference compared to the whole-genome distribution reported  
228 in<sup>11</sup>) (**Fig. 4f; Tables S30-S31; Methods; Supplementary Results ‘Yq12 heterochromatic  
229 subregion’**). No novel SVA (SINE-VNTR-Alu) or HERV (human endogenous retroviruses) elements  
230 were observed within these 43 Y chromosome sequences. Three out of seven LINE-1 insertions are  
231 reported as full-length, including one with two intact ORFs within an intron of the *PCDH11Y* gene,  
232 suggesting that at least one potential retrotransposition-competent polymorphic LINE-1 element resides

233 on the Y chromosome. Among the 25 identified transposable elements, six were shared between  
234 phylogenetically related individuals (including the *Alu* insertion known as the YAP marker fixed in all  
235 haplogroup DE Y chromosomes<sup>23</sup>), while 19 were found in single individuals (**Tables S30-S31**). For  
236 the *Alu* insertions in the Yq12 subregion, we noted that *Alu*Y (denoted as A1 and an A2 in **Fig. 4f**)  
237 insertions have occurred in the proximal and distal regions, respectively, at least 180,000 years ago, and  
238 have subsequently undergone expansions of the *Alu*-containing arrays. Based on these patterns, we can  
239 ascertain arrays and/or repeat units with the same *Alu* insertion are related to each other (**Fig. 4f**). While  
240 the intra-repeat array expansions may be caused by replication slippage, non-allelic homologous  
241 recombination may cause both intra- and inter-array expansion<sup>24,25</sup>, although gene conversion can not  
242 be excluded.

243 Furthermore, the ONT data provides a means to explore the base level epigenetic landscape of  
244 the Y chromosome across these 43 individuals (**Fig. S30**). Here, we focused on DNA methylation at  
245 CpG sites, hereafter referred to as DNAm. We found 2,861 DNAm segments (**Methods**) that vary  
246 across these Y chromosomes (**Fig. S31a; Table S32**). 21% of the variation in DNAm levels is  
247 associated with haplogroups (Permanova  $p=0.003$ ,  $n=41$ ), while only 4.8% of the expression levels  
248 (Permanova  $p=0.005$  ( $n=210$ ), leveraging the Geuvadis RNA-seq expression data<sup>26</sup>) is associated with  
249 haplogroups (**Methods; Supplemental Results ‘Functional analysis’**). There is a significant  
250 association of Y haplogroup with both DNAm and gene expression particularly for five genes (*BCORP*  
251 (**Fig. S32**), *LINC00280*, *LOC100996911*, *PRKY*, *UTY*). Lastly, we find 194 Y-chromosomal genetic  
252 variants, including a 171 base-pair insertion (SV) and one inversion, that impact DNAm levels on  
253 chromosome Y (**Table S33; Supplementary Results ‘Functional analysis’**). Taken together, this  
254 suggests that the genetic background, either on the Y chromosome or elsewhere in the genome, can  
255 impact the functional outcome (the epigenetic and transcriptional profiles) of specific genes on the Y  
256 chromosome.

257

### 258 ***Genetic variation and evolution of the Y-chromosomal heterochromatic regions***

259 *Variation in the size and structure of centromeric/pericentromeric repeat arrays.* Our analysis  
260 of 21 chromosome Y centromeres (17 contiguously assembled centromeres, 3 centromeres with a single  
261 break within the *DYZ3*  $\alpha$ -satellite array without unplaced contigs, and the T2T Y centromere) allowed  
262 the investigation of its diversity and evolution in detail (**Methods**). In general, the chromosome Y  
263 centromeres are composed of 171-bp *DYZ3*  $\alpha$ -satellite repeat units<sup>3</sup>, organized into a higher-order repeat  
264 (HOR) array, flanked on either side by short stretches of monomeric  $\alpha$ -satellite. The monomeric  $\alpha$ -  
265 satellite transitions into a unique sequence on the p-arm and an array of human satellite III (*HSat3*) on  
266 the q-arm.

267 Analysis of each  $\alpha$ -satellite HOR array revealed that it ranges in size from 264 kbp to 1.361  
268 Mbp (mean 667 kbp), with the largest arrays found in samples of African ancestry (mean 900 kbp) and  
269 smaller arrays found in samples of American, European, East Asian, or South Asian ancestry (means



270 664, 488, 264, and 565 kbp, respectively; **Figs. S17, S33; Table S11; Methods**)<sup>27,28</sup>. The *DYZ3*  $\alpha$ -  
271 satellite HOR array is mostly composed of a 34-monomer repeating unit and is the most prevalent HOR  
272 type found in all samples (**Figs. 3e,f**). However, we identified two other HORs that were present at high  
273 frequency among the analyzed Y chromosomes: a 35-monomer HOR found in 14/21 samples and a 36-  
274 monomer HOR found in 11/21 samples (**Methods**). While the 35-monomer HOR is present across  
275 different Y lineages in the Y phylogeny, the 36-monomer HOR has been lost in phylogenetically closely  
276 related Y chromosomes representing the QR haplogroups (**Fig. S33**). Analysis of the sequence  
277 composition of these HORs revealed that the 36-monomer HOR likely represents the ancestral state of  
278 the canonical 35-mer and 34-mer HOR after deletion of the 22nd  $\alpha$ -satellite monomer in the resulting  
279 HORs, respectively (**Fig. 3f; Methods**).

280 The overall organization of the *DYZ3*  $\alpha$ -satellite HOR array is similar to that found on other  
281 human chromosomes, with highly identical  $\alpha$ -satellite HORs in the core of the centromere that become  
282 increasingly divergent towards the periphery<sup>29-32</sup>. There is a directionality of the divergent monomers  
283 at the periphery of the Y centromeres such that a larger block of diverged monomers is consistently  
284 found at the p-arm side of the centromere compared to the block of diverged monomers juxtaposed to  
285 the q-arm.

286 Adjacent to the *DYZ3*  $\alpha$ -satellite HOR array is an *HSat3* repeat array, which ranges in size from  
287 372 to 488 kbp (mean 378 kbp), followed by a *DYZ17* repeat array, which ranges in size from 858 kbp  
288 to 1.740 Mbp (mean 1.085 Mbp). Comparison of the sizes of these three repeat arrays reveals no  
289 significant correlation among their sizes (**Fig. 3e; Figs. S34-S36; Table S11**).

290 The *DYZ19* repeat array is located on the long arm, flanked by X-degenerate regions (**Fig. 1a**)  
291 and composed of 125-bp repeat units (fragment of an LTR) in head-to-tail fashion. It is one of the  
292 subregions which has been completely assembled across all 43 Y chromosomes. It shows the highest  
293 variation in size compared to other chromosome Y subregions, ranging from 65 to 410 kbp (a 6.7-fold  
294 difference). The HG02492 individual (haplogroup J2a) with the smallest-sized *DYZ19* repeat array has  
295 an approximately 200 kbp deletion in this subregion (**Table S11**). In 43/44 Y chromosomes (including  
296 T2T Y), there appears to be evidence of at least two rounds of mutation/expansion (**Fig. 3d**, green and  
297 red colored blocks, respectively, **Figs. S19-21**) leading to directional homogenization of the central and  
298 distal parts of the region in all Y chromosomes. Finally, we have observed a recent ~80 kbp duplication  
299 event shared by the 11 phylogenetically related haplogroup QR samples (**Figs. S19-S21**) which must  
300 have occurred approximately 36,000 years ago (**Figs. 1b, S1**), resulting in substantially larger overall  
301 *DYZ19* subregion in these Y chromosomes.

302 Between the Yq11 euchromatin and the Yq12 heterochromatic subregion, lies the *DYZ18*  
303 subregion. We have found that this subregion comprises 3 distinct repeat arrays: a *DYZ18* repeat array,  
304 a 3.1-kbp repeat array and a 2.7-kbp repeat array (**Figs. S37-S44**). The 3.1-kbp repeat array appears to  
305 be composed of degenerate copies of the *DYZ18* repeat unit, exhibiting 95.8% sequence identity (using  
306 SNVs only) across the length of the repeat unit. The 2.7-kbp repeat array appears to have originated

307 from both the *DYZ18* (23% of the 2.7-kbp repeat unit shows 86.3% sequence identity to *DYZ18*) and  
308 *DYZ1* (77% of the 2.7-kbp repeat unit shows 97% sequence identity to *DYZ1*) repeat units (**Fig. S37**).  
309 All three repeat arrays (*DYZ18*, 3.1-kbp and 2.7-kbp) show a similar pattern and level of methylation  
310 to the *DYZ1* repeat arrays (**Fig. S45**), in that we observe constitutive hypermethylation.

311 *The Yq12 subregion is composed of two alternating repeat arrays that expand and contract*  
312 *considerably but retain a 1:1 monomer repeat unit ratio.* The Yq12 subregion is the most challenging  
313 portion of the Y chromosome to assemble contiguously due to its highly repetitive nature and size. In  
314 this study, we completely assembled the Yq12 subregion for six individuals (HG01890, HG02666,  
315 HG00358, HG01106, HG01952 and HG02011) and compared it to the Yq12 subregion of the T2T Y  
316 chromosome (**Figs. 1a, 4a,f; Tables S10-S11; Supplementary Results ‘Yq12 heterochromatic**  
317 **subregion’**). The largest completely assembled Yq12 subregion is the 7th largest Yq12 subregion  
318 observed among the 44 samples analyzed (**Fig. S15b**). Therefore, the assembly outcome is likely  
319 determined not only by the size of the region. This subregion is composed of alternating arrays of repeat  
320 units: *DYZ1* and *DYZ2*<sup>3,5,33–36</sup>. The *DYZ1* repeat unit is approximately 3.5 kbp and consists mainly of  
321 simple repeats and pentameric satellite sequences, and it has been recently referred to as HSat3A6<sup>4</sup>. The  
322 *DYZ2* repeat (which has also been recently referred to as HSat1B<sup>31</sup>), is approximately 2.4 kbp and  
323 consists mainly of a tandemly repeated AT-rich simple repeat fused to a 5' truncated *Alu* element  
324 followed by an HSATI satellite sequence (**Fig. S37**). The *DYZ1* repeat unit showed more variation in  
325 size (range from 1,165 to 3,608 bp, with 95% of all *DYZ1* repeat units longer than 3,000 bp with a mean  
326 length of 3,543 bp) compared to the *DYZ2* repeat units (range from 1,275 to 3,719 bp, with 93.7% of  
327 all *DYZ2* repeats 2,420 bp in size) (**Methods**).

328 The *DYZ1* repeat units are tandemly arranged into larger *DYZ1* repeat arrays as are the *DYZ2*  
329 repeat units (**Fig. 4**). The total number of *DYZ1* and *DYZ2* arrays (range from 34 to 86, mean: 61) were  
330 significantly positively correlated (Spearman Correlation=0.90, p-value=0.0056, n=7, alpha=0.05) with  
331 the total length of the analyzed Yq12 region (**Fig. S46**). Whereas the length of the individual *DYZ1* and  
332 *DYZ2* repeat arrays were found to be widely variable (**Fig. 4b; Fig. S47**). The *DYZ1* arrays were  
333 significantly longer (range from 50,420 to 3,599,754 bp, mean: 535,314 bp) than the *DYZ2* arrays (range  
334 from 11,215 to 2,202,896 bp, mean: 354,027 bp, two-tailed Mann-Whitney U test (n=7) p-value < 0.05)  
335 (**Fig. 4b**). The *DYZ1* and *DYZ2* arrays alternate with one another but interestingly the total number of  
336 *DYZ1* and *DYZ2* repeat units is nearly equal within each individual Y chromosome assembly (*DYZ1* to  
337 *DYZ2* ratio ranges from 0.88 to 1.33, mean: 1.09, SD: 0.17) (**Fig. 4b; Table S34**). From ONT data, we  
338 have observed a consistent hypermethylation of the *DYZ2* repeat arrays compared to the *DYZ1* repeat  
339 arrays, the sequence composition of the two repeats is markedly different in terms of CG content (24%  
340 *DYZ2* versus 38% *DYZ1*) and number of CpG dinucleotides (1 CpG/150 bp *DYZ2* versus 1 CpG/35 bp  
341 *DYZ1*) potentially explaining the marked DNA methylation differences (**Fig. S30**).

342 Sequence analysis of the repeat units in Yq12 suggests that the *DYZ1* and *DYZ2* repeat arrays  
343 and the entire Yq12 subregion may have evolved in a similar manner, and similarly to the centromeric

344 region (see above). Specifically, when examining repeat units within a given repeat array, the repeat  
345 units near the middle of the repeat array show a higher level of sequence similarity to each other than  
346 to the repeat units at the distal regions of the repeat arrays (**Fig. 4d; Fig. S48**). This suggests that  
347 expansion and contraction tends to occur in the middle of the repeat arrays, homogenizing these units  
348 but allowing divergent repeat units to accumulate towards the periphery. Similarly, when looking at the  
349 entire Yq12 subregion, we observed that entire repeat arrays located in the middle of the Yq12 subregion  
350 tend to be more similar in sequence to each other than to repeat arrays at the periphery (**Fig. 4e; Figs.**  
351 **S48-S49**). This observation is supported by results from the *DYZ2* repeat divergence analysis and the  
352 inter-*DYZ2* array profile comparison (**Methods**).

## 353 Discussion

354 The mammalian Y chromosome has been notoriously difficult to assemble owing to its  
355 extraordinarily high repeat content. Here, we present the Y-chromosomal assemblies of 43 males from  
356 the 1000 Genomes Project dataset and a comprehensive analysis of their genetic and epigenetic  
357 variation and composition. While both the GRCh38 Y and the T2T Y represent relatively recently  
358 emerged (TMRCA 54.5 kya (95% HPD interval: 47.6 - 62.4 kya), **Fig. S1**) European Y lineages, 49%  
359 of our Y chromosomes carry African Y lineages, including two of the deepest rooting human Y lineages  
360 (A0b and A1a, TMRCA 183 kya (95% HPD interval: 160-209 kya)) which we have assembled  
361 contiguously allowing us to investigate how the Y chromosome has changed over 180,000 years of  
362 human evolution.

363 For the first time, we have been able to comprehensively and precisely examine the extent of  
364 genetic variation down to the nucleotide level across multiple human Y chromosomes. The male-  
365 specific region of the Y chromosome can be roughly divided into two portions: the euchromatic and the  
366 heterochromatic regions. Within the euchromatic region, the single-copy protein-coding Y-  
367 chromosomal genes, present in the GRCh38 Y reference sequence, are conserved in all 43 Y assemblies  
368 with few single nucleotide polymorphisms. 5/8 copy-number variable protein-coding gene families  
369 located in the ampliconic subregions showed variation in terms of copy number, with the highest  
370 variation determined in the *TSPY* gene family (from 24 to 40 copies, **Table S23**).

371 The euchromatic region harbors considerable structural variation across the 43 individuals.  
372 Most notably, we identified 14 inversions that affect half of the Y-chromosomal euchromatin, with only  
373 the most closely related pair of African Ys (from NA19317 and NA19347) showing the exact same  
374 inversion composition. We have been able to narrow down the breakpoints for all of the inversions, and  
375 for 8 of 14 inversions have refined the breakpoints down to a 500-bp region. The determination of the  
376 molecular mechanism causing the inversions remains challenging; however, the increased recurrent  
377 inversion rate on the Y chromosome compared to the rest of the human genome may be in part due to  
378 DNA double-strand breaks being repaired by intra-chromatid recombination<sup>37</sup>. Since inversions

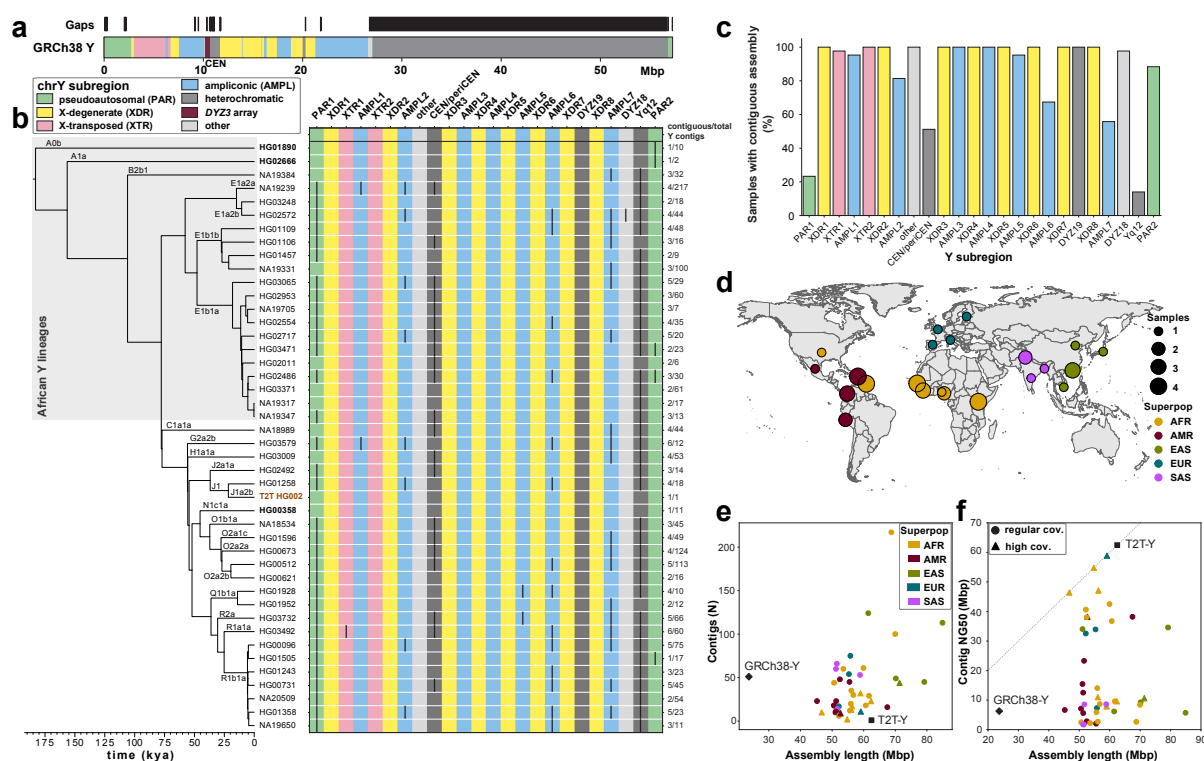
379 generally suppress interchromosomal recombination events<sup>38</sup>, and the Y chromosome is paired with the  
380 X chromosome during meiosis, the widespread presence of inversions on the Y chromosome is  
381 consistent with limiting synaptonemal complexes to a small portion at the termini of the Y chromosome  
382 (i.e., PAR1 and PAR2). A neutral evolutionary view of the ubiquitousness of the inversions on the Y  
383 chromosome would be that inversions can arise anywhere in the genome but often lead to the formation  
384 of disadvantageous variants at chromosome regions that are normally involved in recombination.  
385 Therefore, most inversions would be lost by selection over time except for those in the non-recombining  
386 portions of the Y chromosome, where they are more tolerated and can therefore accumulate.

387         There are 4 heterochromatic subregions in the human Y chromosome: the (peri-)centromeric  
388 region, *DYZ18*, *DYZ19* and Yq12. Heterochromatin is usually defined by the preponderance of highly  
389 repetitive sequences and the constitutive dense packaging of the chromatin within<sup>39</sup>. When we examined  
390 the DNA sequence and the methylation patterns for these 4 heterochromatic subregions, the high content  
391 of the repetitive sequences and the high level of methylation (**Figs. S30, S45**) observed is consistent  
392 with the definition of heterochromatin. Furthermore, resolving the complete structural variation in the  
393 heterochromatic regions of the human Y chromosome provides novel molecular archeological evidence  
394 for evolutionary mechanisms. For example, in this study we have shown how the higher order structure  
395 at the centromeric region of the Y chromosome has evolved from an ancestral 36-mer HOR to a 34-mer  
396 HOR which predominates in the centromeres of current human males<sup>40</sup>. Moreover, the degeneration of  
397 these repeat units of the (peri-)centromeric region of the Y chromosome has a directional bias towards  
398 the p-arm side. The presence of an *Alu* element right at the q-arm boundary, but not on the p-arm side,  
399 raises the possibility that following two *Alu* insertions, over 180,000 years ago, led to a subsequent *Alu*-  
400 *Alu* recombination that deleted the region in between and removing the diverged centromeric sequence  
401 block<sup>41</sup>. In the Yq12 subregion, there appear to be localized expansions and contractions of the *DYZ1*  
402 and *DYZ2* repeat units; however, evolutionary constraints seem to dictate a need to preserve the nearly  
403 1:1 ratio of these two repeat units among all males studied by an unknown mechanism. These alternating  
404 repeat units are confined between two inversions that are fixed among modern-day humans.

405         In this study, we have fully sequenced and analyzed 43 diverse Y chromosomes and identified  
406 the full extent of variation of this chromosome across more than 180,000 years of human evolution. For  
407 the first time, sequence-level resolution across multiple human Y chromosomes has revealed new DNA  
408 sequences, new elements of conservation and provided molecular data that give us important insights  
409 into genomic stability and chromosomal integrity. Ultimately, the ability to effectively assemble the  
410 complete human Y chromosome has been a long-awaited yet crucial milestone towards understanding  
411 the full extent of human genetic variation and provides the starting point to associate Y-chromosomal  
412 sequences to specific human traits and more thoroughly study human evolution.

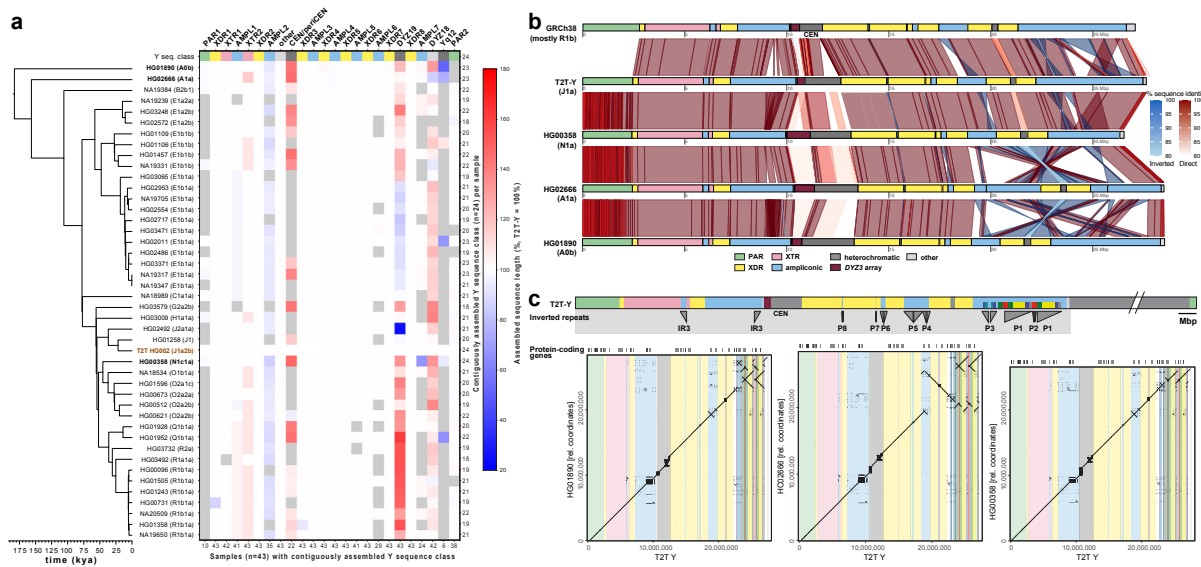
413

## 414 Main figures



415  
 416 **Figure 1.** Assemblies capture more diversity and are more complete than the GRCh38 Y sequence.  
 417 **a.** Human Y chromosome structure based on the GRCh38 Y reference sequence.  
 418 **b.** Phylogenetic relationships (left) with haplogroup labels of the analyzed Y chromosomes with branch  
 419 lengths drawn proportional to the estimated times between successive splits (see **Fig. S1** and **Table**  
 420 **S1** for additional details). Summary of Y chromosome assembly completeness (right) with black lines  
 421 representing non-contiguous assembly of that region (**Methods**). Numbers on the right indicate the  
 422 number of Y contigs needed to achieve the indicated contiguity/total number of assembled Y contigs for  
 423 each sample). CEN - centromere - includes the *DYZ3*  $\alpha$ -satellite array and the pericentromeric region.  
 424 Three contiguously assembled Y chromosomes are in bold (assemblies for HG02666 and HG00358 are  
 425 contiguous from telomere to telomere, while HG01890 assembly has a break approx. 100 kbp before  
 426 the end of PAR2) and the T2T Y for HG002 in brown. Note - GRCh38 Y sequence mostly represents  
 427 haplogroup R1b.  
 428 **c.** The proportion of contiguously assembled Y-chromosomal subregions across 43 samples.  
 429 **d.** Geographic origin and sample size of the included 1000 Genomes Project samples colored according  
 430 to the continental groups (AFR, African; AMR, American; EUR, European; SAS, South Asian; EAS,  
 431 East Asian).  
 432 **e.** Y-chromosomal assembly length vs number of Y contigs. Gap sequences (N's) were excluded from  
 433 GRCh38.  
 434 **f.** Y-chromosomal assembly length vs Y contig NG50. High coverage defined as >50X genome-wide  
 435 PacBio HiFi read depth. Gap sequences (N's) were excluded from GRCh38.

436



437

438 **Figure 2.** Size and structural variation of Y chromosomes.

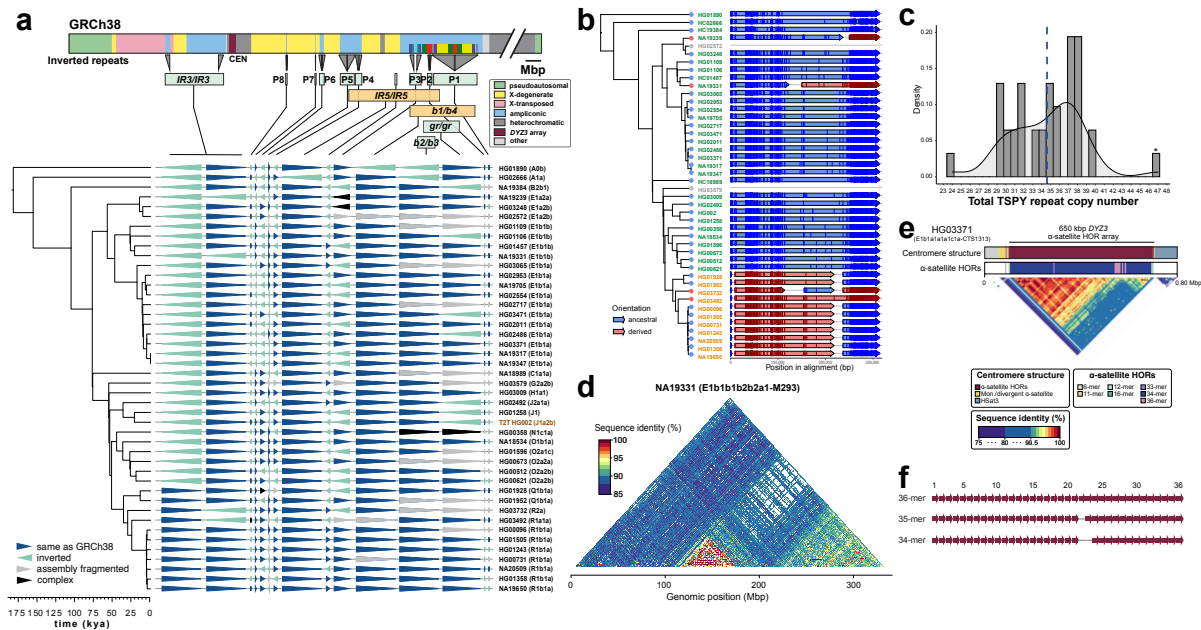
439 **a.** Size variation of contiguously assembled Y-chromosomal subregions shown as a heatmap relative  
 440 to the T2T Y size (as 100%). Boxes in gray indicate regions not contiguously assembled (**Methods**).  
 441 Numbers on the bottom indicate contiguously assembled samples for each subregion out of a total of 43  
 442 samples, and numbers on the right indicate the contiguously assembled Y subregions out of 24 regions  
 443 for each sample.

444 **b.** Comparison of the three contiguously assembled Y chromosomes to GRCh38 and the T2T Y  
 445 (excluding Yq12 and PAR2 subregions).

446 **c.** Dotplots of three contiguously assembled Y chromosomes vs the T2T Y (excluding Yq12 and PAR2),  
 447 annotated with Y subregions and segmental duplications in ampliconic subregion 7 (see **Fig. S22** for  
 448 details).

449

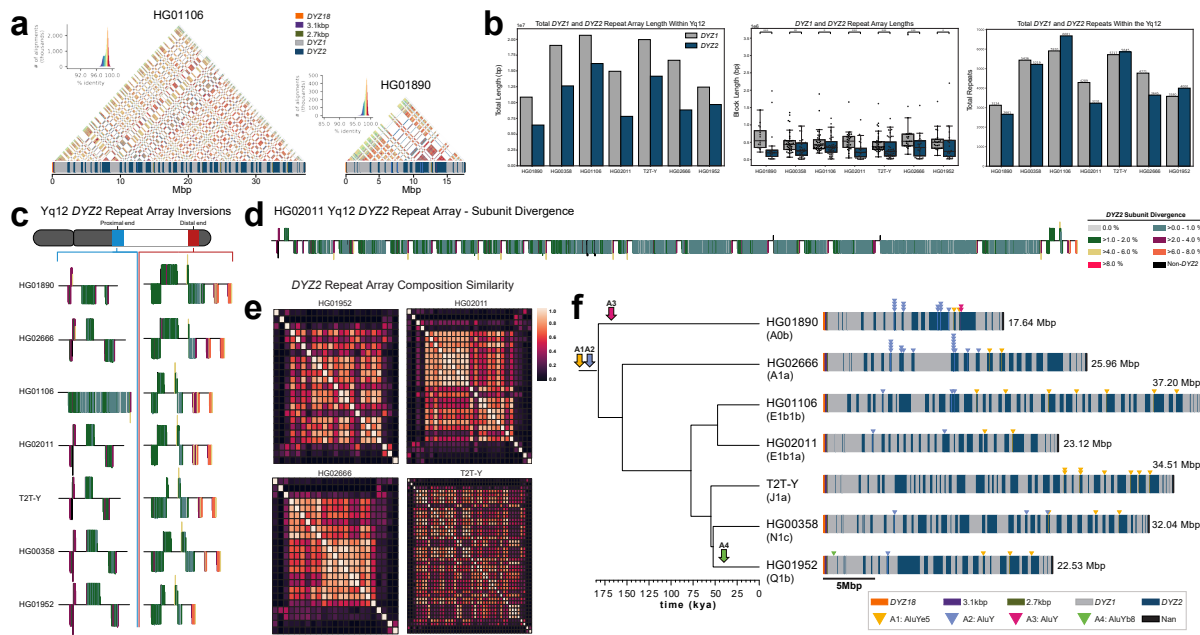
450



451

452 **Figure 3.** Characterization of large SVs.

453 **a.** Distribution of 14 euchromatic inversions in phylogenetic context, with the schematic of the GRCh38  
 454 Y structure shown above, annotated with Y subregions, inverted repeat locations and segmental  
 455 duplications in ampliconic subregion 7 (see **Fig. S22** for details). Inverted segments are indicated below  
 456 as green (recurrent) and orange (singleton events) boxes. **b.** Inversion breakpoint identification in the IR3  
 457 repeats. Samples highlighted in orange color have undergone two inversions (**Fig. S57, Supplementary**  
 458 **Results ‘Y-chromosomal Inversions’**). The red tip colors in the phylogenetic tree indicate samples  
 459 which have undergone an additional inversion and therefore carry the region between IR3 repeats in  
 460 inverted orientation compared to samples with blue tip. Informative PSV positions are shown as vertical  
 461 lines with darker color in each of the arrows. The orange dotted line indicates the start of the unique  
 462 ‘spacer’ region. Any information that is not available is indicated by gray. **c.** The total copy number  
 463 distribution of the TSPY gene across 39 samples (T2T Y is marked with an asterisk). **d.** Sequence  
 464 identity heatmap of the *DYZI9* repeat array from NA19331 (using 1 kbp window size) highlighting the  
 465 higher sequence similarity within central and distal regions. **e.** Genetic landscape of the chromosome Y  
 466 centromeric region from HG03371. This centromere harbors the newly identified ancestral 36-monomer  
 467 HORs, from which the canonical 34-monomer HOR is derived. **f.** The 34-monomer  $\alpha$ -satellite HOR  
 468 was formed via two sequential steps in which a single  $\alpha$ -satellite monomer residing at the 22nd position  
 469 was deleted. The 34-monomer  $\alpha$ -satellite HOR dominates all chromosome Y centromeres.



470

471 **Figure 4.** Yq12 heterochromatic region.

472 **a.** Yq12 heterochromatic subregion sequence identity heatmap in 5-kbp windows for HG01106 and  
 473 HG01890 with repeat array annotations.

474 **b.** Bar plot of the total length of *DYZ1* and *DYZ2* repeat arrays for each sample (left), boxplots of  
 475 individual array lengths (middle) and the total number of *DYZ1* and *DYZ2* repeat units (right) within  
 476 contiguously assembled genomes. Black dots represent individual arrays and stars (\*) denote a  
 477 statistically significant difference between *DYZ1* and *DYZ2* array lengths (two-sided Mann-Whitney U  
 478 test: p-value < 0.05, alpha=0.05, Methods).

479 **c.** *DYZ2* repeat array inversions in the proximal and distal ends of the Yq12 region. *DYZ2* repeats are  
 480 colored based on their divergence estimate (see panel d) and visualized based on their orientation (sense  
 481 - up, antisense - down).

482 **d.** Detailed representation of *DYZ2* subunit divergence estimates for HG02011. Length of each line is a  
 483 function of the subunit length. Orientation (sense - up, antisense - down).

484 **e.** Heatmaps showing the inter-*DYZ2* repeat array subunit composition similarity within a sample.  
 485 Similarity is calculated using the Bray-Curtis index (1 – Bray-Curtis Distance, 1.0 = exactly the same  
 486 composition). *DYZ2* repeat arrays are shown in physical order from proximal to distal (from top down,  
 487 and from left to right).

488 **f.** Mobile element insertions identified in the Yq12 subregion highlighting four putative *Alu* insertions,  
 489 their locations, and insertion occurrences across the seven complete genomes. The total size of Yq12  
 490 region is indicated on the right.

491



## 492 Methods

### 493 1. Sample selection

494 Samples were selected from the 1000 Genomes Project Diversity Panel<sup>42</sup> and at least one  
495 representative was selected from each of 26 populations (**Table S1**). 13/28 samples were included from  
496 the Human Genome Structural Variation Consortium (HGSVC) Phase 2 dataset, which was published  
497 previously<sup>11</sup>. In addition, for 15/28 samples data was newly generated as part of the HGSVC efforts  
498 (see the section ‘Data production’ for details). We also included 15 samples from the Human  
499 Pangenome Reference Consortium (HPRC) (**Table S1**).

### 500 2. Data production

#### 501 a. PacBio HiFi sequence production

502 **University of Washington** - Sample HG00731 data have been previously described<sup>11</sup>. Additional  
503 samples HG02554 and HG02953 were prepared for sequencing in the same way but with the following  
504 modifications: isolated DNA was sheared using the Megaruptor 3 instrument (Diagenode) twice using  
505 settings 31 and 32 to achieve a peak size of ~15-20 kbp. The sheared material was subjected to  
506 SMRTbell library preparation using the Express Template Prep Kit v2 and SMRTbell Cleanup Kit v2  
507 (PacBio). After checking for size and quantity, the libraries were size-selected on the Pippin HT  
508 instrument (Sage Science) using the protocol “0.75% Agarose, 15-20 kbp High Pass” and a cutoff of  
509 14-15 kbp. Size-selected libraries were checked via fluorometric quantitation (Qubit) and pulse-field  
510 sizing (FEMTO Pulse). All cells were sequenced on a Sequel II instrument (PacBio) using 30-hour  
511 movie times using version 2.0 sequencing chemistry and 2-hour pre-extension. HiFi/CCS analysis was  
512 performed using SMRT Link v10.1 using an estimated read-quality value of 0.99.

513 **The Jackson Laboratory** - High-molecular-weight (HMW) DNA was extracted from 30M frozen  
514 pelleted cells using the Gentra Puregene extraction kit (Qiagen). Purified gDNA was assessed using  
515 fluorometric (Qubit, Thermo Fisher) assays for quantity and FEMTO Pulse (Agilent) for quality. For  
516 HiFi sequencing, samples exhibiting a mode size above 50 kbp were considered good candidates.  
517 Libraries were prepared using SMRTBell Express Template Prep Kit 2.0 (Pacbio). Briefly, 12 µl of  
518 DNA was first sheared using gTUBEs (Covaris) to target 15-18 kbp fragments. Two 5 µg of sheared  
519 DNA were used for each prep. DNA was treated to remove single strand overhangs, followed by DNA  
520 damage repair and end repair/ A-tailing. The DNA was then ligated V3 adapter and purified using  
521 Ampure beads. The adapter ligated library was treated with Enzyme mix 2.0 for Nuclease treatment to  
522 remove damaged or non-intact SMRTbell templates, followed by size selection using Pippin HT

523 generating a library that has a size >10 kbp. The size selected and purified >10 kbp fraction of libraries  
524 were used for sequencing on Sequel II (Pacbio).

## 525 b. ONT-UL sequence production

526 **University of Washington** - High-molecular-weight (HMW) DNA was extracted from 2 aliquots of 30  
527 M frozen pelleted cells using phenol-chloroform approach as described in<sup>43</sup>. Libraries were prepared  
528 using Ultra long DNA Sequencing Kit (SQK-ULK001, ONT) according to the manufacturer's  
529 recommendation. Briefly, DNA from ~10M cells was incubated with 6 µl of fragmentation mix (FRA)  
530 at room temperature (RT) for 5 min and 75°C for 5 min. This was followed by an addition of 5 µl of  
531 adaptor (RAP-F) to the reaction mix and incubated for 30 min at RT. The libraries were cleaned up  
532 using Nanobind disks (Circulomics) and Long Fragment Buffer (LFB) (SQK-ULK001, ONT) and  
533 eluted in Elution Buffer (EB). Libraries were sequenced on the flow cell R9.4.1 (FLO-PRO002, ONT)  
534 on a PromethION (ONT) for 96 hrs. A library was split into 3 loads, with each load going 24 hrs  
535 followed by a nuclease wash (EXP-WSH004, ONT) and subsequent reload.

536 **The Jackson Laboratory** - High-molecular-weight (HMW) DNA was extracted from 60 M frozen  
537 pelleted cells using phenol-chloroform approach as previously described<sup>44</sup>. Libraries were prepared  
538 using Ultra long DNA Sequencing Kit (SQK-ULK001, ONT) according to the manufacturer's  
539 recommendation. Briefly, 50ug of DNA was incubated with 6 µl of FRA at RT for 5 min and 75°C for  
540 5 min. This was followed by an addition of 5 µl of adaptor (RAP-F) to the reaction mix and incubated  
541 for 30 min at RT. The libraries were cleaned up using Nanodisks (Circulomics) and eluted in EB.  
542 Libraries were sequenced on the flow cell R9.4.1 (FLO-PRO002, ONT) on a PromethION (ONT) for  
543 96 hrs. A library was generally split into 3 loads with each loaded at an interval of about 24 hrs or when  
544 pore activity dropped to 20%. A nuclease wash was performed using Flow Cell Wash Kit (EXP-  
545 WSH004) between each subsequent load.

## 546 c. Bionano optical genome maps production

547 Optical mapping data were generated at Bionano Genomics, San Diego, USA. Lymphoblastoid  
548 cell lines were obtained from Coriell Cell Repositories and grown in RPMI 1640 media with 15% FBS,  
549 supplemented with L-glutamine and penicillin/streptomycin, at 37°C and 5% CO<sub>2</sub>. Ultra-high-  
550 molecular-weight DNA was extracted according to the Bionano Prep Cell Culture DNA Isolation  
551 Protocol(Document number 30026, revision F) using a Bionano SP Blood & Cell DNA Isolation Kit  
552 (Part #80030). In short, 1.5 M cells were centrifuged and resuspended in a solution containing  
553 detergents, proteinase K, and RNase A. DNA was bound to a silica disk, washed, eluted, and  
554 homogenized via 1hr end-over-end rotation at 15 rpm, followed by an overnight rest at RT. Isolated  
555 DNA was fluorescently tagged at motif CTTAAG by the enzyme DLE-1 and counter-stained using a  
556 Bionano Prep™ DNA Labeling Kit – DLS (catalog # 8005) according to the Bionano Prep Direct Label

557 and Stain (DLS) Protocol(Document number 30206, revision G). Data collection was performed using  
558 Saphyr 2nd generation instruments (Part #60325) and Instrument Control Software (ICS) version  
559 4.9.19316.1.

#### 560 d. Strand-seq data generation and data processing

561 Strand-seq data were generated at EMBL and the protocol is as follows. EBV-transformed  
562 lymphoblastoid cell lines from the 1000 Genomes Project (Coriell Institute; **Table S1**) were cultured in  
563 BrdU (100 uM final concentration; Sigma, B9285) for 18 or 24 hrs, and single isolated nuclei (0.1%  
564 NP-40 substitute lysis buffer<sup>45</sup> were sorted into 96-well plates using the BD FACSMelody and BD  
565 Fusion cell sorter. In each sorted plate, 94 single cells plus one 100-cell positive control and one 0-cell  
566 negative control were deposited. Strand-specific single-cell DNA sequencing libraries were generated  
567 using the previously described Strand-seq protocol<sup>45,46</sup> and automated on the Beckman Coulter Biomek  
568 FX P liquid handling robotic system<sup>47</sup>. Following 15 rounds of PCR amplification, 288 individually  
569 barcoded libraries (amounting to three 96-well plates) were pooled for sequencing on the Illumina  
570 NextSeq500 platform (MID-mode, 75 bp paired-end protocol). The demultiplexed FASTQ files were  
571 aligned to the GRCh38 reference assembly (GCA\_000001405.15) using BWA aligner (version 0.7.15-  
572 0.7.17) for standard library selection. Aligned reads were sorted by genomic position using SAMtools  
573 (version 1.10) and duplicate reads were marked using sambamba (version 1.0). Low-quality libraries  
574 were excluded from future analyses if they showed low read counts (<50 reads per Mbp), uneven  
575 coverage, or an excess of ‘background reads’ (reads mapped in opposing orientation for chromosomes  
576 expected to inherit only Crick or Watson strands) yielding noisy single-cell data, as previously  
577 described<sup>45</sup>. Aligned BAM files were used for inversion discovery as described in<sup>22</sup>.

#### 578 e. Hi-C data production

579 Lymphoblastoid cell lines were obtained from Coriell Cell Repositories and cultured in RPMI  
580 1640 supplemented with 15% FBS. Cells were maintained at 37°C in an atmosphere containing 5%  
581 CO<sub>2</sub>. Hi-C libraries using 1.5 M human cells as input were generated with Proximo Hi-C kits v4.0  
582 (Phase Genomics, Seattle, WA) following the manufacturer’s protocol with the following modification:  
583 in brief, cells were crosslinked, quenched, lysed sequentially with Lysis Buffers 1 and 2, and liberated  
584 chromatin immobilized on magnetic recovery beads. A 4-enzyme cocktail composed of DpnII (GATC),  
585 DdeI (CTNAG), HinfI (GANTC), and MseI (TTAA) was used during the fragmentation step to improve  
586 coverage and aid haplotype phasing. Following fragmentation and fill-in with biotinylated nucleotides,  
587 fragmented chromatin was proximity ligated for 4 hrs at 25°C. Crosslinks were then reversed, DNA  
588 purified and biotinylated junctions recovered using magnetic streptavidin beads. Bead-bound proximity  
589 ligated fragments were then used to generate a dual-unique indexed library compatible with Illumina  
590 sequencing chemistry. The Hi-C libraries were evaluated using fluorescent-based assays, including

591 qPCR with the Universal KAPA Library Quantification Kit and TapeStation (Agilent). Sequencing of  
592 the libraries was performed at New York Genome Center (NYGC) on an Illumina Novaseq 6000  
593 instrument using 2x150 bp cycles.

#### 594 f. RNAseq data production

595 Total RNA of cell pellets were isolated using QIAGEN RNeasy Mini Kit according to the  
596 manufacturer's instructions. Briefly, each cell pellet (10 M cells) was homogenized and lysed in Buffer  
597 RLT Plus, supplemented with 1%  $\beta$ -mercaptoethanol. The lysate-containing RNA was purified using  
598 an RNeasy spin column, followed by an in-column DNase I treatment by incubating for 10 min at RT,  
599 and then washed. Finally, total RNA was eluted in 50  $\mu$ L RNase-free water. RNA-seq libraries were  
600 prepared with 300 ng total RNA using KAPA RNA Hyperprep with RiboErase (Roche) according to  
601 the manufacturer's instructions. First, ribosomal RNA was depleted using RiboErase. Purified RNA was  
602 then fragmented at 85°C for 6 min, targeting fragments ranging 250-300 bp. Fragmented RNA was  
603 reverse transcribed with an incubation of 25°C for 10 min, 42°C for 15 min, and an inactivation step at  
604 70°C for 15 min. This was followed by a second strand synthesis and A-tailing at 16°C for 30 min,  
605 62°C for 10 min. The double-stranded cDNA A-tailed fragments were ligated with Illumina unique dual  
606 index adapters. Adapter-ligated cDNA fragments were then purified by washing with AMPure XP  
607 beads (Beckman). This was followed by 10 cycles of PCR amplification. The final library was cleaned  
608 up using AMPure XP beads. Quantification of libraries was performed using real-time qPCR (Thermo  
609 Fisher). Sequencing was performed on an Illumina NovaSeq platform generating paired end reads of  
610 100 bp at The Jackson Laboratory for Genomic Medicine.

#### 611 g. Iso-seq data production

612 Iso-seq data were generated at The Jackson Laboratory. Total RNA was extracted from 10 M  
613 human cell pellets. 300 ng total RNA were used to prepare Iso-seq libraries according to Iso-seq Express  
614 Template Preparation (Pacbio). First, full-length cDNA was generated using NEBNext Single Cell/  
615 Low Input cDNA synthesis and Amplification Module in combination with Iso-seq Express Oligo Kit.  
616 Amplified cDNA was purified using ProNex beads. The cDNA yield of 160–320 ng then underwent  
617 SMRTbell library preparation including a DNA damage repair, end repair, and A-tailing and finally  
618 ligated with Overhang Barcoded Adapters. Libraries were sequenced on Pacbio Sequel II. Iso-seq reads  
619 were processed with default parameters using the PacBio Iso-seq3 pipeline.

### 620 3. Construction and dating of Y phylogeny

621 The genotypes were jointly called from the 1000 Genomes Project Illumina high-coverage data  
622 from <sup>48</sup> using the ~10.4 Mbp of chromosome Y sequence previously defined as accessible to short-read  
623 sequencing<sup>49</sup>. BCFtools (v1.9)<sup>50,51</sup> was used with minimum base quality and mapping quality 20,

624 defining ploidy as 1, followed by filtering out SNVs within 5 bp of an indel call (Snpgap) and removal  
625 of indels. Additionally, we filtered for a minimum read depth of 3. If multiple alleles were supported  
626 by reads, then the fraction of reads supporting the called allele should be  $\geq 0.85$ ; otherwise, the genotype  
627 was converted to missing data. Sites with  $\geq 6\%$  of missing calls, i.e., missing in more than 3 out of 44  
628 samples, were removed using VCFtools (v0.1.16)<sup>52</sup>. After filtering, a total of 10,406,108 sites remained,  
629 including 12,880 variant sites. Since Illumina short-read data was not available from two samples,  
630 HG02486 and HG03471, data from their fathers (HG02484 and HG03469, respectively) was used for  
631 Y phylogeny construction and dating.

632 The Y haplogroups of each sample were predicted as previously described<sup>15</sup> and correspond to  
633 the International Society of Genetic Genealogy nomenclature (ISOGG, <https://isogg.org>, v15.73,  
634 accessed in August 2021). We used the coalescence-based method implemented in BEAST (v1.10.4)<sup>53</sup>  
635 to estimate the ages of internal nodes in the Y phylogeny. A starting maximum likelihood phylogenetic  
636 tree for BEAST was constructed with RAxML (v8.2.10)<sup>54</sup> with the GTRGAMMA substitution model.  
637 Markov chain Monte Carlo samples were based on 200 million iterations, logging every 1000 iterations.  
638 The first 10% of iterations were discarded as burn-in. A constant-sized coalescent tree prior, the GTR  
639 substitution model, accounting for site heterogeneity (gamma) and a strict clock with a substitution rate  
640 of  $0.76 \times 10^{-9}$  (95% confidence interval:  $0.67 \times 10^{-9}$ – $0.86 \times 10^{-9}$ ) single-nucleotide mutations per bp  
641 per year was used<sup>55</sup>. A prior with a normal distribution based on the 95% confidence interval of the  
642 substitution rate was applied. A summary tree was produced using TreeAnnotator (v1.10.4) and  
643 visualized using the FigTree software (v1.4.4).

644 The closely related pair of African E1b1a1a1a-CTS8030 lineage Y chromosomes carried by  
645 NA19317 and NA19347 differ by 3 SNVs across the 10,406,108 bp region, with the TMRCA estimated  
646 to 200 ya (95% HPD interval: 0 - 500 ya).

647 A separate phylogeny (see **Fig. 4f**) was reconstructed using seven samples (HG01890,  
648 HG02666, HG01106, HG02011, T2T Y from NA24385/HG002, HG00358 and HG01952) with  
649 contiguously assembled Yq12 region following identical approach to that described above, with a single  
650 difference that sites with any missing genotypes were filtered out. The final callset used for phylogeny  
651 construction and split time estimates using Beast contained a total of 10,382,177 sites, including 5,918  
652 variant sites.

## 653 4. *De novo* Assembly Generation

### 654 a. Reference assemblies

655 We used the GRCh38 (GCA\_000001405.15) and the CHM13 (GCA\_009914755.3) plus the  
656 T2T Y assembly from GenBank (CP086569.2) released in April 2022. We note that we did not use the  
657 unlocalised GRCh38 contig “chrY\_KI270740v1\_random” (37,240 bp, composed of 289 *DYZ19*  
658 primary repeat units) in any of the analyses presented in this study.

## 659 b. Constructing *de novo* assemblies

660 All 28 HGSVC and 15 HPRC samples were processed with the same Snakemake<sup>56</sup> workflow  
661 (see “Code Availability” statement in main text) to first produce a *de novo* whole-genome assembly  
662 from which selected sequences were extracted in downstream steps of the workflow. The *de novo*  
663 whole-genome assembly was produced using Verkko v1.0<sup>18</sup> with default parameters, combining all  
664 available PacBio HiFi and Oxford Nanopore data per sample to create a whole-genome assembly:

```
665 verkko -d work_dir/ --hifi {hifi_reads} --nano {ont_reads}
```

666 We note here that we had to manually modify the assembly FASTA file produced by Verkko  
667 for the sample NA19705 for the following reason: at the time of assembly production, the Verkko  
668 assembly for the sample NA19705 was affected by a minor bug in Verkko v1.0 resulting in an empty  
669 output sequence for contig “0000598”. The Verkko development team suggested removing the affected  
670 record, i.e. the FASTA header plus the subsequent blank line, because the underlying bug is unlikely to  
671 affect the overall quality of the assembly. We followed that advice, and continued the analysis with the  
672 modified assembly FASTA file. Our discussion with the Verkko development team is publicly  
673 documented in the Verkko Github issue #66. The assembly FASTA file was adapted as follows:

```
674 egrep -v "(^$|unassigned\ -0000598)" assembly.original.fasta >  
675 assembly.fasta
```

676 For the samples with at least 50X HiFi input coverage (termed high-coverage samples, **Tables**  
677 **S1-S2**), we generated alternative assemblies using hifiasm v0.16.1-r375<sup>57</sup> for quality control purposes.  
678 Hifiasm was executed with default parameters using only HiFi reads as input, thus producing partially  
679 phased output assemblies “hap1” and “hap2” (cf. hifiasm documentation):

```
680 hifiasm -o {out_prefix} -t {threads} {hifi_reads}
```

681 The two hifiasm haplotype assemblies per sample are comparable to the Verkko assemblies in that they  
682 represent a diploid human genome without further identification of specific chromosomes, i.e., the  
683 assembled Y sequence contigs have to be identified in a subsequent process that we implemented as  
684 follows.

685 We employed a simple rule-based strategy to identify and extract assembled sequences for the  
686 two quasi-haploid chromosomes X and Y. The following rules were applied in the order stated here:

687 Rule 1: the assembled sequence has primary alignments only to the target sequence of interest, i.e. to  
688 either chrY or chrX. The sequence alignments were produced with minimap2 v2.24<sup>58</sup>:

```
689 minimap2 -t {threads} -x asm20 -Y --secondary=yes -N 1 --cs -c --paf-  
690 no-hit
```

691 Rule 2: the assembled sequence has mixed primary alignments, i.e. not only to the target sequence of  
692 interest, but exhibits Y-specific sequence motif hits for any of the following motifs: *DYZ1*, *DYZ18* and  
693 the secondary repeat unit of *DYZ3* from<sup>3</sup>. The motif hits were identified with HMMER v3.3.2.dev  
694 (commit hash #016cba0)<sup>59</sup>:

```
695 nhmmer --cpu {threads} --dna -o {output_txt} --tblout {output_table}  
696 -E 1.60E-150 {query_motif} {assembly}
```

697 Rule 3: the assembled sequence has mixed primary alignments, i.e. not only to the target sequence of  
698 interest, but exhibits more than 300 hits for the Y-unspecific repeat unit *DYZ2* (see Section ‘**Yq12 *DYZ2***  
699 **Consensus and Divergence**’ for details on *DYZ2* repeat unit consensus generation). The threshold was  
700 determined by expert judgement after evaluating the number of motif hits on other reference  
701 chromosomes. The same HMMER call as for rule 2 was used with an E-value cutoff of 1.6e-15 and a  
702 score threshold of 1700.

703 Rule 4: the assembled sequence has no alignment to the chrY reference sequence, but exhibits Y-  
704 specific motif hits as for rule 2.

705 Rule 5: the assembled sequence has mixed primary alignments, but more than 90% of the assembled  
706 sequence (in bp) has a primary alignment to a single target sequence of interest; this rule was introduced  
707 to resolve ambiguous cases of primary alignments to both chrX and chrY.

708 After identification of all assembled chrY and chrX sequences, the respective records were  
709 extracted from the whole-genome assembly FASTA file and, if necessary, reverse-complemented to be  
710 in the same orientation as the T2T reference using custom code.

## 711 c. Assembly evaluation and validation

### 712 Error detection in *de novo* assemblies

713 Following established procedures<sup>11,18</sup>, we implemented two independent approaches to identify  
714 regions of putative misassemblies for all 43 samples. First, we used VerityMap (v2.1.1-alpha-dev  
715 #8d241f4)<sup>19</sup> that generates and processes read-to-assembly alignments to flag regions in the assemblies  
716 that exhibit spurious signal, i.e., regions of putative assembly errors, but that may also indicate  
717 difficulties in the read alignment. Given the higher accuracy of HiFi reads, we executed VerityMap only  
718 with HiFi reads as input:

```
719  
720 python repos/VerityMap/veritymap/main.py --no-reuse --reads  
721 {hifi_reads} -t {threads} -d hifi -l SAMPLE-ID -o {out_dir}  
722 {assembly_FASTA}
```

723 Second, we used DeepVariant (v1.3.0)<sup>60</sup> and the PEPPER-Margin-DeepVariant pipeline (v0.8,  
724 DeepVariant v1.3.0,<sup>61</sup>) to identify heterozygous (HET) SNVs using both HiFi and ONT reads aligned  
725 to the *de novo* assemblies. Given the quasi-haploid nature of the chromosome Y assemblies, we counted  
726 all HET SNVs remaining after quality filtering (bcftools v1.15 “filter” QUAL>=10) as putative  
727 assembly errors:

```
728 /opt/deepvariant/bin/run_deepvariant --model_type="PACBIO" --  
729 ref={assembly_FASTA} --num_shards={threads} --reads={HiFi-to-
```

```
730 assembly_BAM} --sample_name=SAMPLE-ID --output_vcf={out_vcf} --  
731 output_gvcf={out_gvcf} --intermediate_results_dir=$TMPDIR  
732  
733 run_pepper_margin_deepvariant call_variant --bam {ONT-to-  
734 assembly_BAM} --fasta {assembly_FASTA} --output_dir {out_dir} --  
735 threads {threads} --ont_r9_guppy5_sup --sample_name SAMPLE-ID --  
736 output_prefix {out_prefix} --skip_final_phased_bam --gvcf
```

737 The output of all error detection steps was merged using custom code (see “Code Availability”  
738 statement in main text; **Table S8**).

739

740 Assembly QV estimates were produced with yak v0.1 ([github.com/lh3/yak](https://github.com/lh3/yak)) following the examples in  
741 its documentation (see readme in referenced repository). The QV estimation process requires an  
742 independent sequence data source to derive a (sample-specific) reference k-mer set to compare the k-  
743 mer content of the assembly. In our case, we used available short read data to create said reference k-  
744 mer set, which necessitated excluding the samples HG02486 and HG03471 because no short reads were  
745 available. For the chromosome Y-only QV estimation, we restricted the short reads to those with  
746 primary alignments to our Y assemblies or to the T2T-Y, which we added during the alignment step to  
747 capture reads that would align to Y sequences missing from our assemblies.

#### 748 Assembly evaluation using Bionano Genomics optical mapping data

749 To evaluate the accuracy of Verkko assemblies, all samples (n=43) were first *de novo*  
750 assembled using the raw optical mapping molecule files (bnx), followed by alignment of assembled  
751 contigs to the T2T whole genome reference genome assembly (CHM13 + T2T Y) using Bionano Solve  
752 (v3.5.1) pipelineCL.py.

```
753 python2.7 Solve3.5.1_01142020/Pipeline/1.0/pipelineCL.py -T 64 -U -j  
754 64 -jpb 64 -N 6 -f 0.25 -i 5 -w -c 3 \  
755 -y \  
756 -b ${ bnx} \  
757 -l ${output_dir} \  
758 -t Solve3.5.1_01142020/RefAligner/1.0/ \  
759 -a  
760 Solve3.5.1_01142020/RefAligner/1.0/optArguments_haplotype_DLE1_saphy  
761 r_human.xml \  
762 -r ${ref}
```

763 To improve the accuracy of optical mapping Y chromosomal assemblies, unaligned molecules,  
764 molecules that align to T2T chromosome Y and molecules that were used for assembling contigs but  
765 did not align to any chromosomes were extracted from the optical mapping *de novo* assembly results.



766 These molecules were used for the following three approaches: 1) local *de novo* assembly using Verkko  
767 assemblies as the reference using pipelineCL.py, as described above; 2) alignment of the molecules to  
768 Verkko assemblies using refAligner (Bionano Solve (v3.5.1)); and 3) hybrid scaffolding using optical  
769 mapping *de novo* assembly consensus maps (cmaps) and Verkko assemblies by hybridScaffold.pl.

```
770 perl Solve3.5.1_01142020/HybridScaffold/12162019/hybridScaffold.pl \  
771 -n ${fastafilename} \  
772 -b ${bionano_cmap} \  
773 -c  
774 Solve3.5.1_01142020/HybridScaffold/12162019/hybridScaffold_DLE1_conf  
775 ig.xml \  
776 -r Solve3.5.1_01142020/RefAligner/1.0/RefAligner \  
777 -o ${output_dir} \  
778 -f -B 2 -N 2 -x -y \  
779 -m ${bionano_bnx} \  
780 -p Solve3.5.1_01142020/Pipeline/12162019/ \  
781 -q  
782 Solve3.5.1_01142020/RefAligner/1.0/optArguments_nonhaplotype_DLE1_sa  
783 phyr_human.xml
```

784 Inconsistencies between optical mapping data and Verkko assemblies were identified based on  
785 variant calls from approach 1 using “exp\_refineFinal1\_merged\_filter\_inversions.smap” output file.  
786 Variants were filtered out based on the following criteria: a) variant size smaller than 500 base pairs; b)  
787 variants labeled as “heterozygous”; c) translocations with a confidence score of  $\leq 0.05$  and inversions  
788 with a confidence score of  $\leq 0.7$  (as recommended on Bionano Solve Theory of Operation: Structural  
789 Variant Calling - Document Number: 30110); d) variants with a confidence score of  $< 0.5$ . Variant  
790 reference start and end positions were then used to evaluate the presence of single molecules which  
791 span the entire variant using alignment results from approach 2. Alignments with a confidence score of  
792  $< 30.0$  were filtered out. Hybrid scaffolding results, conflict sites provided in “conflicts\_cut\_status.txt”  
793 output file from approach 3 were used to evaluate if inconsistencies identified above based on optical  
794 mapping variant calls overlap with conflict sites (i.e. sites identified by hybrid scaffolding pipeline  
795 representing inconsistencies between sequencing and optical mapping data) (**Table S35**). Furthermore,  
796 we used molecule alignment results to identify coordinate ranges on each Verkko assembly which had  
797 no single DNA molecule coverage using the same alignment confidence score threshold of 30.0, as  
798 described above, dividing assemblies into 10 kbp bins and counting the number single molecules  
799 covering each 10 kbp window (**Table S36**).

#### 800 d. *De novo* assembly annotation

##### 801 Annotation of Y-chromosomal subregion

802 The 24 Y-chromosomal subregion coordinates (**Table S9**) relative to the GRCh38 reference  
803 sequence were obtained from<sup>7</sup>. Since Skov et al. produced their annotation on the basis of a coordinate  
804 liftover from GRCh37, we updated some coordinates to be compatible with the following publicly  
805 available resources: for the pseudoautosomal regions we used the coordinates from the UCSC Genome  
806 Browser for GRCh38.p13 as they slightly differed. Additionally, Y-chromosomal amplicon start and  
807 end coordinates were edited according to more recent annotations from<sup>62</sup>, and the locations of *DYZ19*  
808 and *DYZ18* repeat arrays were adjusted based on the identification of their locations using HMMER3  
809 (v3.3.2)<sup>63</sup> with the respective repeat unit consensus sequences from<sup>3</sup>.

810 The locations and orientations of Y-chromosomal subregions in the T2T Y were determined by  
811 mapping the subregion sequences from the GRCh38 Y to the T2T Y using minimap2 (v2.24, see above).  
812 The same approach was used to determine the subregion locations in each *de novo* assembly with  
813 subregion sequences from both GRCh38 and the T2T Y (**Table S9**). The locations of the *DYZ18* and  
814 *DYZ19* repeat arrays in each *de novo* assembly were further confirmed (and coordinates adjusted if  
815 necessary) by running HMMER3 (see above) with the respective repeat unit consensus sequences  
816 from<sup>3</sup>. Only tandemly organized matches with HMMER3 score thresholds higher than 1700 for *DYZ18*  
817 and 70 for *DYZ19*, respectively, were included and used to report the locations and sizes of these repeat  
818 arrays.

819 A Y-chromosomal subregion was considered as contiguous if it was assembled contiguously  
820 from the subclass on the left to the subclass on the right (note that the *DYZ18* subregion is completely  
821 deleted in HG02572), except for PAR regions where they were defined as >95% length of the T2T Y  
822 PAR regions and with no unplaced contigs. Note that due to the requirement of no unplaced contigs the  
823 assembly for HG02666 appears to have a break in PAR2 subregion, while it is contiguously assembled  
824 from the telomeric sequence of PAR1 to telomeric sequence in PAR2 without breaks (however, there  
825 is a ~14 kbp unplaced PAR2 contig aligning best to a central region of PAR2). The assembly of  
826 HG01890 however has a break approximately 100 kbp before the end of PAR2. Assembly of PAR1  
827 remains especially challenging due to its sequence composition and sequencing biases<sup>8,10</sup>, and among  
828 our samples was contiguously assembled for 10/43 samples, while PAR2 was contiguously assembled  
829 for 39/43 samples.

##### 830 Annotation of centromeric and pericentromeric regions

831 To annotate the centromeric regions, we first ran RepeatMasker (v4.1.0) on 26 Y-chromosomal  
832 assemblies (22 samples with contiguously assembled pericentromeric regions, 3 samples with a single  
833 gap and no unplaced centromeric contigs, and the T2T Y) to identify the locations of  $\alpha$ -satellite repeats  
834 using the following command:

```
835 RepeatMasker -species human -dir {path_to_directory} -pa  
836 {num_of_threads} {path_to_fasta}
```

837 Then, we subsetting each contig to the region containing  $\alpha$ -satellite repeats and ran HumAS-  
838 HMMER (v3.3.2; [https://github.com/fedorrik/HumAS-HMMER\\_for\\_AnVIL](https://github.com/fedorrik/HumAS-HMMER_for_AnVIL)) to identify the location  
839 of  $\alpha$ -satellite higher-order repeats (HORs), using the following command:

```
840 Hmmer-run.sh {directory_with_fasta} AS-HORs-hmmer3.0-  
841 170921.hmm {num_of_threads}
```

842 We combined the outputs from RepeatMasker (v4.1.0) and HumAS-HMMER to generate a  
843 track that annotates the location of  $\alpha$ -satellite HORs and monomeric or diverged  $\alpha$ -satellite within each  
844 centromeric region.

845 To determine the size of the  $\alpha$ -satellite HOR array, we used the  $\alpha$ -satellite HOR annotations  
846 generated via HumAS-HMMER (v3.3.2; described above) to determine the location of *DYZ3*  $\alpha$ -satellite  
847 HORs, focusing on only those HORs annotated as “live” (e.g. S4CYH1L). Live HORs are those that  
848 have a clear higher-order pattern and are highly (>90%) homogenous<sup>64</sup>. This analysis was conducted  
849 on 21 centromeres (including the T2T Y), excluding 5/26 samples (NA19384, HG01457, HG01890,  
850 NA19317, NA19331), where, despite a contiguously assembled pericentromeric subregion, the  
851 assembly contained unplaced centromeric contig(s).

852 To annotate the human satellite III (*HSat3*) and *DYZ17* arrays within the pericentromere, we  
853 ran StringDecomposer (v1.0.0) on each assembly centromeric contig using the *HSat3* and *DYZ17*  
854 consensus sequences described in Altemose, 2022, Seminars in Cell and Developmental Biology<sup>65</sup> and  
855 available at the following URL:  
856 [https://github.com/altemose/HSatReview/blob/main/Output\\_Files/HSat123\\_consensus\\_sequences.fa](https://github.com/altemose/HSatReview/blob/main/Output_Files/HSat123_consensus_sequences.fa)

857 We ran the following command:

```
858 stringdecomposer/run_decomposer.py {path_to_contig_fasta}  
859 {path_to_consensus_sequence+fasta} -t {num_of_threads} -o  
860 {output_tsv}
```

861 The *HSat3* array was determined as the region that had a sequence identity of 60% or greater,  
862 while the *DYZ17* array was determined as the region that had a sequence identity of 65% or greater.

## 863 5. Downstream analysis

### 864 a. Effect of input read depth on assembly contiguity

865 We explored a putative dependence between the characteristics of the input read sets, such as  
866 read length N50 or genomic coverage, and the resulting assembly contiguity by training multivariate  
867 regression models (“ElasticNet” from scikit-learn v1.1.1, see “Code Availability” statement in main  
868 text). The models were trained following standard procedures with 5-fold nested cross-validation (see  
869 scikit-learn documentation for “ElasticNetCV”). We note that we did not use the haplogroup

870 information due to the unbalanced distribution of haplogroups in our dataset. We selected basic  
871 characteristics of both the HiFi and ONT-UL input read sets (read length N50, mean read length,  
872 genomic coverage and genomic coverage for ONT reads exceeding 100 kbp in length, i.e., the so-called  
873 ultralong fraction of ONT reads; **Table S38**) as model features and assembly contig NG50, assembly  
874 length or number of assembled contigs as target variable.

875

## 876 b. Locations of assembly gaps

877 The assembled Y-chromosomal contigs were mapped to the GRCh38 and the CHM13 plus  
878 T2T-Y reference assemblies using minimap2 with the flags `-x asm20 -Y -p 0.95 --`  
879 `secondary=yes -N 1 -a -L --MD --eqx`. The aligned Y-chromosomal sequences for each  
880 reference were partitioned to 1 kbp bins to investigate assembly gaps. Gap presence was inferred in bins  
881 where the average read depth was either lower or higher than 1. To investigate the potential factors  
882 associated with gap presence, we analyzed these sequences to compare the GC content, segmental  
883 duplication content, and Y subregion. Read depth for each bin was calculated using mosdepth<sup>66</sup> and the  
884 flags `-n -x`. GC content for each bin was calculated using BedTools `nuc` function<sup>67</sup>. Segmental  
885 duplication locations for GRCh38 Y were obtained from the UCSC genome browser, and for the  
886 CHM13 plus T2T Y from<sup>2</sup>. Y-chromosomal subregion locations were determined as described in  
887 Methods section ‘*De novo* assembly annotation with Y-chromosomal subregions’. The bin read depth  
888 and GC content statistics were merged into matrices and visualized using *matplotlib* and *seaborn*<sup>68,69</sup>.

889

## 890 c. Effect of read depth on assembly contiguity

891 Read depth statistics of both PacBio HiFi and ONT raw reads as mapped to the *de novo*  
892 assemblies were calculated using samtools bedcov (version 1.15.1)<sup>50</sup>. We investigated normality  
893 through histograms and qq-plotting of the read depth distribution, and proceeded to use the mean read  
894 depth in our analyses. Average read depth for the whole Y- chromosomal assembly was regressed  
895 against contig N50 and L50, total contig number, total assembly length, and largest contig length.  
896 Regressions were calculated using the OLS function in *statsmodels*, and visualized using *matplotlib* and  
897 *seaborn*<sup>68-70</sup>.

898

## 899 d. Comparison of assembled Y subregion sizes across samples

900 Sizes for each chromosome’s (peri-)centromeric regions were obtained as described in Methods  
901 section ‘Annotation of pericentromeric regions’. The size variation of (peri-)centromeric regions (*DYZ3*  
902 alpha-satellite array, *Hsat3*, *DYZ17* array, and total (peri-)centromeric region), and the *DYZ19*, *DYZ18*  
903 and *TSPY* repeat arrays were compared across samples using a heatmap, incorporating phylogenetic  
904 context. The sizes of the (peri-)centromeric regions (*DYZ3* alpha-satellite array, *Hsat3* and *DYZ17*

905 array) were regressed against each other using the OLS function in *statsmodels*, and visualized using  
906 *matplotlib* and *seaborn*<sup>68</sup>.

907

## 908 e. Comparison and visualization of *de novo* assemblies

909 The similarities of three contiguously assembled Y chromosomes (HG00358, HG02666,  
910 HG01890), including comparison to both GRCh38 and the T2T Y, was assessed using *blastn*<sup>71</sup> with  
911 sequence identity threshold of 80% (95% threshold was used for PAR1 subregion) (**Fig. 2b**) and  
912 excluding non-specific alignments (i.e. showing alignments between different Y subregions), followed  
913 by visualization with *genoPlotR* (0.8.11)<sup>72</sup>. Y subregions were uploaded as DNA segment files and  
914 alignment results were uploaded as comparison files following the file format recommended by the  
915 developers of the *genoplots* package. Unplaced contigs were excluded, and all Y-chromosomal  
916 subregions, except for Yq12 heterochromatic region and PAR2, were included in queries.

```
917 blastn -query $file1 -subject $file2 -subject_besthit -outfmt '7  
918 qstart qend sstart send qseqid sseqid pident length mismatch gaps  
919 evalue bitscore sstrand qcovs qcovhsp qlen slen' -out  
920 ${outputfile}.out
```

921

```
922 plot_gene_map(dna_segs=dnaSegs, comparisons=comparisonFiles,  
923 xlims=xlims, legend = TRUE, gene_type = "headless_arrows",  
924 dna_seg_scale=TRUE, scale=FALSE)
```

925 For other samples, three-way comparisons were generated between the GRCh38 Y, Verkko *de*  
926 *novo* assembly and the T2T Y sequences, removing alignments with less than 80% sequence identity.  
927 The similarity of closely related NA19317 and NA19347 Y-chromosomal assemblies was assessed  
928 using the same approach.

929

## 930 f. Sequence identity heatmaps

931 Sequence identity within repeat arrays was investigated by running *StainedGlass*<sup>73</sup>. For the  
932 centromeric regions, *StainedGlass* was run with the following configuration: `window = 5785` and  
933 `mm_f = 30000`. We adjusted the color scale in the resulting plot using a custom R script that redefines  
934 the breaks in the histogram and its corresponding colors. This script is publicly available here:  
935 [https://eichlerlab.gs.washington.edu/help/glogsdon/Shared\\_with\\_Pille/StainedGlass\\_adjustedScale.R](https://eichlerlab.gs.washington.edu/help/glogsdon/Shared_with_Pille/StainedGlass_adjustedScale.R).

936 The command used to generate the new plots is: `StainedGlass_adjustedScale.R -b`  
937 `{output_bed} -p {plot_prefix}`. For the *DYZ19* repeat array, `window =`  
938 `1000` and `mm_f = 10000` were used, 5 kbp of flanking sequence was included from both sides,  
939 followed by adjustment of color scale using the custom R script (see above).

940 For the Yq12 subregion (including the *DYZ18* repeat array), `window = 5000` and `mm_f`  
941 `= 10000` were used, and 10 kbp of flanking sequence was included. In addition to samples with  
942 contiguously assembled Yq12 subregion, the plots were generated for two samples (NA19705 and  
943 HG01928) with a single gap in Yq12 subregion (the two contigs containing Yqhet sequence were joined  
944 into a single contig with 100 Ns added to the joint location). HG01928 contains a single unplaced Yqhet  
945 contig (approximately 34 kbp in size) which was not included. For the Yq11/Yq12 transition region,  
946 100 kbp proximal to the *DYZ18* repeat and 100 kbp of the first *DYZ1* repeat array was included in the  
947 StainedGlass runs, using `window = 2000` and `mm_f = 10000`.

948

#### 949 g. Dotplot generation

950 Dotplot visualizations were created using the NAHRwhals package version 0.9 which provides  
951 visualization utilities and a custom pipeline for pairwise sequence alignment based on minimap2 (v2.24)  
952 . Briefly, NAHRwhals initiates pairwise alignments by splitting long sequences into chunks of 1 - 10  
953 kbp which are then aligned to the target sequence separately, enhancing the capacity of minimap2 to  
954 correctly capture inverted or repetitive sequence alignments. Subsequently, alignment pairs are  
955 concatenated whenever the endpoint of one alignment falls in close proximity to the startpoint of another  
956 (base pair distance cutoff: 5% of the chunk length). Pairwise alignment dotplots are created with a  
957 pipeline based on the ggplot2 package, with optional .bed files accepted for specifying colorization or  
958 gene annotation. The NAHRwhals package and further documentation are available at  
959 <https://github.com/WHops/nahrchainer>, and dotplot views of selected regions can be accessed at  
960 [http://ftp.1000genomes.ebi.ac.uk/vol1/ftp/data\\_collections/HGSVC2/working/20221020\\_Dotplots\\_ch](http://ftp.1000genomes.ebi.ac.uk/vol1/ftp/data_collections/HGSVC2/working/20221020_Dotplots_ch)  
961 [rY\\_ASMS](#)

962

#### 963 h. Inversion analyses

##### 964 Inversion calling using Strand-seq data

965 The inversion calling from Strand-seq data, available for 30/43 samples and the T2T Y, using  
966 both the GRCh38 and the T2T Y sequences as references was performed as described previously<sup>22</sup>.

967 Note on the P5 palindrome spacer direction in the T2T Y assembly: the P5 spacer region is  
968 present in the same orientation in both GRCh38 (where the spacer orientation had been chosen  
969 randomly, see Supplementary Figure 11 from<sup>3</sup> for more details) and the T2T Y sequence, while high-  
970 confidence calls from the Strand-seq data from individual HG002/NA24385 against both the GRCh38  
971 and T2T Y report it to be in inverted orientation. It is therefore likely that the P5 spacer orientations are  
972 incorrect in both GRCh38 Y and the T2T Y and in the P5 inversion recurrence estimates we therefore  
973 considered HG002/NA24385 to carry the P5 inversion (as shown on **Fig. 3a**, inverted relative to  
974 GRCh38).

## 975 Inversion calling from the *de novo* assemblies

976 In order to determine the inversions from the *de novo* assemblies, we aligned the Y-  
977 chromosomal repeat units/segmental duplications as published by <sup>62</sup> to the *de novo* assemblies as  
978 described above (see Section: ‘Annotation with Y-chromosomal subregions’). Inverted alignment  
979 orientation of the unique sequences flanked by repeat units/segmental duplications relative to the  
980 GRCh38 Y was considered as evidence of inversion. The presence of inversions was further confirmed  
981 by visual inspection of *de novo* assembly dotplots generated against both GRCh38 and T2T Y sequences  
982 (see Methods section: Dotplot generation), followed by merging with the Strand-seq calls (**Table S26**).

## 983 Inversion rate estimation

984 In order to estimate the inversion rate, we counted the minimum number of inversion events  
985 that would explain the observed genotype patterns in the Y phylogeny (**Fig. 3a**). A total of 12,880 SNVs  
986 called in the set of 44 males and Y chromosomal substitution rate from above (see Methods section  
987 ‘Construction and dating of Y phylogeny’) was used. A total of 126.4 years per SNV mutation was then  
988 calculated  $(0.76 \times 10^{-9} \times 10,406,108 \text{ bp})^{-1}$ , and converted into generations assuming a 30-year generation  
989 time<sup>74</sup>. Thus each SNV corresponds to 4.21 generations, translating into a total branch length of 54,287  
990 generations for the 44 samples. For a single inversion event in the phylogeny this yields a rate of  $1.84$   
991  $\times 10^{-5}$  (95% CI:  $1.62 \times 10^{-5}$  to  $2.08 \times 10^{-5}$ ) mutations per father-to-son Y transmission. The confidence  
992 interval of the inversion rate was obtained using the confidence interval of the SNV rate.

## 993 Determination of inversion breakpoint ranges

994 We focussed on the following eight recurrent inversions to narrow down the inversion  
995 breakpoint locations: IR3/IR3, IR5/IR5, and palindromes P8, P7, P6, P5, P4 and P3 (**Fig. 3a**), and  
996 leveraged the ‘phase’ information (i.e. proximal/distal) of paralogous sequence variants (PSVs) across  
997 the segmental duplications mediating the inversions as follows. First, we extracted proximal and distal  
998 inverted repeat sequences flanking the identified inversions (spacer region) and aligned them using  
999 MAFFT (v7.487)<sup>75,76</sup> with default parameters. From the alignment, we only selected informative sites  
1000 (i.e. not identical across all repeats and samples), excluding singletons and removing sites within  
1001 repetitive or poorly aligned regions as determined by Tandem Repeat Finder (v4.09.1)<sup>77</sup> and Gblocks  
1002 (v0.91b)<sup>78</sup>, respectively. We inferred the ancestral state of the inverted regions following the maximum  
1003 parsimony principle as follows: we counted the number of inversion events that would explain the  
1004 distribution of inversions in the Y phylogeny by assuming a) that the reference (i.e. same as GRCh38  
1005 Y) state was ancestral and b) that the inverted (i.e. inverted compared to GRCh38 Y) state was ancestral.  
1006 The definition of ancestral state for each of the regions was defined as the lesser number of events to  
1007 explain the tree (IR3: reference; IR5: reference; P8: inverted; P7: reference; P5: reference; P4:  
1008 reference; P3: reference). As we observed a clear bias of inversion state in both African (Y lineages A,  
1009 B and E) and non-African Y lineages for the P6 palindrome (the African Y lineages have more inverted

1010 states (17/21) and non-African Y lineages have more reference states (17/23)), we determined the  
1011 ancestral state and inversion breakpoints for African and non-African Y lineages separately in the  
1012 following analyses.

1013 We then defined an ancestral group as any samples showing an ancestral direction in the spacer  
1014 region, and selected sites that have no overlapping alleles between the proximal and distal alleles in the  
1015 defined ancestral group, which were defined as the final set of informative PSVs. For IR3, we used the  
1016 ancestral group as samples with Y-chromosomal structure 1 (i.e. with the single ~20.3 kbp TSPY repeat  
1017 located in the proximal IR3 repeat) and ancestral direction in the spacer region. According to the allele  
1018 information from the PSVs, we determined the phase (proximal or distal) for each PSV across samples.  
1019 Excluding non-phased PSVs (e.g. the same alleles were found in both proximal and distal sequences),  
1020 any two adjacent PSVs with the same phase were connected as a segment while masking any single  
1021 PSVs with a different phase from the flanking ones to only retain reliable contiguous segments. An  
1022 inversion breakpoint was determined to be a range where phase switching occurred between two  
1023 segments, and the coordinate was converted to the T2T Y coordinate based on the multiple sequence  
1024 alignment and to the GRCh38 Y coordinate using the LiftOver tool at the UCSC Genome Browser web  
1025 page (<https://genome.ucsc.edu/cgi-bin/hgLiftOver>). Samples with non-contiguous assembly of the  
1026 repeat regions were excluded from each analysis of the corresponding repeat region.

1027

## 1028 i. Variant calling

### 1029 Variant calling using *de novo* assemblies

1030 Variants were called from assembly contigs using PAV (v2.1.0)<sup>11</sup> with default parameters using  
1031 minimap2 (v2.17) contig alignments to GRCh38 (primary assembly only,  
1032 [ftp://ftp.1000genomes.ebi.ac.uk/vol1/ftp/data\\_collections/HGSVC2/technical/reference/20200513\\_hg](ftp://ftp.1000genomes.ebi.ac.uk/vol1/ftp/data_collections/HGSVC2/technical/reference/20200513_hg38_NoALT/)  
1033 [38\\_NoALT/](ftp://ftp.1000genomes.ebi.ac.uk/vol1/ftp/data_collections/HGSVC2/technical/reference/20200513_hg38_NoALT/)). Supporting variant calls were done against the same reference with PAV (v2.1.0) using  
1034 LRA<sup>79</sup> alignments (commit e20e67) with assemblies, PBSV (v2.8.0)  
1035 (<https://github.com/PacificBiosciences/pbsv>) with PacBio HiFi reads, SVIM-asm (v1.0.2)<sup>80</sup> with  
1036 assemblies, Sniffles (v2.0.7)<sup>81</sup> with PacBio HiFi and ONT, DeepVariant (v1.1.0)<sup>60,82</sup> with PacBio HiFi,  
1037 Clair3 (v0.1.12)<sup>83</sup> with ONT, CuteSV (v2.0.1)<sup>84</sup> with ONT, and LongShot (v0.4.5)<sup>85</sup> with ONT. A  
1038 validation approach based on the subseq command was used to search for raw-read support in PacBio  
1039 HiFi and ONT<sup>11</sup>.

1040 A merged callset was created from the PAV calls with minimap2 alignments across all samples  
1041 with SV-Pop<sup>11,86</sup> to create a single non-redundant callset. We used merging parameters  
1042 “nr::exact:ro(0.5):szro(0.5,200)” for SV and indel insertions and deletions (Exact size  
1043 & position, then 50% reciprocal overlap, then 50% overlap by size and within 200 bp),  
1044 “nr::exact:ro(0.2)” for inversions (Exact size & position, then 20% reciprocal overlap), and



1045 “nrsnv::exact” for SNVs (exact position and REF/ALT match). The PAV minimap2 callset was  
1046 intersected with each orthogonal support source using the same merging parameters. SVs were accepted  
1047 into the final callset if they had support from two orthogonal sources with at least one being another  
1048 caller (i.e. support from only subseq PacBio HiFi and subseq ONT was not allowed). Indels and SNVs  
1049 were accepted with support from one orthogonal caller. Inversions were manually curated using  
1050 dotplots.

1051 To search for likely duplications within insertion calls, insertion sequences were re-mapped to  
1052 the reference with minimap2 (v2.17) with parameters “-x asm20 -H --secondary=no -r 2k  
1053 -Y -a --eqx -L -t 4”.

1054 To evaluate whether the identified additional *RBMY1B* copies were functional the insertion  
1055 sequence containing the *RBMY1B* duplicate copy was aligned to the reference with minimap2 using  
1056 default parameters. Small variants between the duplicate and reference copy were identified using the  
1057 alignment (CIGAR string parsing). A VCF was generated for these variants and run with VEP (version  
1058 107). Variants VEP annotated with MODIFIER were discarded.

1059 In order to compare the SNV densities between chromosomes the following approach was used:  
1060 for autosomes and chrX, we obtained a set of filtered SNV calls and PAV callable regions from a set of  
1061 32 samples derived from long-read phased assemblies<sup>11</sup>. We used a similar callset generated for chrY  
1062 from this study and separated the pseudoautosomal regions (PAR), which recombine with chrX during  
1063 meiosis, and the MSY, which does not recombine with chrX. For each chromosome, we generated  
1064 globally callable loci by taking a union of all the PAV callable loci (regions where variants could be  
1065 called). To further guarantee that SNVs were not a result of alignment artifacts, we removed simple  
1066 repeats, segmental duplications, N-gaps, and centromeres using UCSC browser tracks. We also  
1067 excluded unreliable regions used to filter the Ebert callset  
1068 ([http://ftp.1000genomes.ebi.ac.uk/vol1/ftp/data\\_collections/HGSVC2/technical/filter/20210127\\_Low](http://ftp.1000genomes.ebi.ac.uk/vol1/ftp/data_collections/HGSVC2/technical/filter/20210127_Low)  
1069 *ConfidenceFilter*/), which is mostly covered by the other region filters from UCSC tracks. We then  
1070 counted the number of SNVs in these callable regions and divided by the callable size in kbp to obtain  
1071 the number of SNVs per kbp. We tested the significance of the difference in means using Welch’s t-test  
1072 by comparing the MSY to all other regions (including PAR and chrX) and by comparing chrX to all  
1073 other regions (including PAR and MSY). The maximum p-value reported for each of these two tests  
1074 was Bonferroni-corrected by multiplying the p-value by the number of other chromosomes tested.

## 1075 Validation of large SVs using optical mapping data

1076 Orthogonal support for merged PAV calls were evaluated by using optical mapping data (**Table**  
1077 **S39**). Molecule support was evaluated using local *de novo* assembly maps which aligned to GRCh38  
1078 reference assembly. This evaluation included all 10 called inversions, and insertions and deletions at  
1079 least 5 kbp or larger in size. Although variants <5 kbp could be resolved by optical mapping technique,

1080 there were loci without any fluorescent labels which could lead to misinterpretation of the results.  
1081 Variant reference (GRCh38) start and end positions were used to evaluate the presence of single  
1082 molecules which span the variant breakpoints using alignment results using Bionano Access (v1.7).  
1083 Alignments with a confidence score of < 30.0 were filtered out.

#### 1084 TSPY repeat array copy number analysis

1085 To perform a detailed analysis of the TSPY repeat array, known to be highly variable in copy  
1086 number<sup>87</sup>, the consensus sequence of the repeat unit was first constructed as follows. The repeat units  
1087 were determined from the T2T Y sequence, the individual repeat unit sequences extracted and aligned  
1088 using MAFFT (v7.487)<sup>75,76</sup> with default parameters. A consensus sequence was generated using  
1089 EMBOSS cons (v6.6.0.0) command line version with default parameters, followed by manual editing  
1090 to replace sites defined as ‘N’s with the major allele across the repeat units. The constructed TSPY  
1091 repeat unit consensus sequence was 20,284 bp.

1092 The consensus sequence was used to identify TSPY repeat units from each *de novo* assembly  
1093 using HMMER3 v3.3.2<sup>63</sup>, excluding five samples (HG03065, NA19239, HG01258, HG00096,  
1094 HG03456) with non-contiguous assembly of this region. TSPY repeat units from each assembly were  
1095 aligned using MAFFT as described above, followed by running HMMER functions “esl-alistat” and  
1096 “esl-alipid” to obtain sequence identity statistics (**Table S13**).

1097

#### 1098 j. Mobile element insertion analysis

##### 1099 Mobile element insertion (MEI) calling

1100 We leveraged an enhanced version of PALMER (Pre-mAsking Long reads for Mobile Element  
1101 insertion,<sup>88</sup>) to detect MEIs across the long-read sequences. Reference-aligned (to both GRCh38 Y and  
1102 T2T Y) Y contigs from Verkko assembly were used as input. Putative insertion sequences of non-  
1103 reference repetitive elements (L1s, Alus or SVAs) were identified based on a library of mobile element  
1104 sequences after a pre-masking process. PALMER then identifies the hallmarks of retrotransposition  
1105 events for the putative insertion signals, including TSD motifs, transductions, and poly(A) tract  
1106 sequences, and etc. Further manual inspection was carried out based on the information of large  
1107 inversions, structural variations, heterochromatic regions, and concordance with the Y phylogeny. Low  
1108 confidence calls overlapping with large SVs or discordant with the Y phylogeny were excluded, and  
1109 high confidence calls were annotated with further genomic content details.

1110 In order to compare the ratios of non-reference mobile element insertions from the Y  
1111 chromosome to the rest of the genome the following approach was used. The size of the GRCh38 Y  
1112 reference of 57.2 Mbp was used, while the total GRCh38 reference sequence length is 3.2 Gbp. At the  
1113 whole genome level, this results in a ratio for non-reference Alu of 0.459 per Mbp (1470/3.2 Gbp) and

1114 for non-reference LINE-1 of 0.066 per Mbp (210/3.2 Gbp)<sup>11</sup>. In chromosome Y, the ratio for non-  
1115 reference Alu and LINE-1 is 0.315 per Mbp (18/57.2 Mbp) and 0.122 per Mbp (7/57.2 Mbp),  
1116 respectively. The ratios within the MEI category were compared using the Chi-square test.

1117

## 1118 k. Gene annotation

### 1119 Genome Annotation - liftoff

1120 Genome annotations of chromosome Y assemblies were obtained by using T2T Y and GRCh38  
1121 Y gff annotation files using liftoff<sup>89</sup>.

```
1122 liftoff -db $dbfile -o $outputfile.gff -u $outputfile.unmapped -dir  
1123 $outputdir -p 8 -m $minimap2dir -sc 0.85 -copies $fastafilename -cds  
1124 $refassembly
```

1125 To evaluate which of the GRCh38 Y protein-coding genes were not detected in Verkko assemblies, we  
1126 selected genes which were labeled as “protein\_coding” from the GENCODEv41 annotation file (i.e., a  
1127 total of 63 protein-coding genes).

1128

## 1129 l. Methylation analysis

1130 Read-level CpG DNA-methylation (DNAm) likelihood ratios were estimated using  
1131 nanopolish version 0.11.1. Nanopolish (<https://github.com/jts/nanopolish>) was run on the alignment to  
1132 GRCh38, for the three complete assemblies (HG00358, HG01890, HG02666) we additionally mapped  
1133 the reads back to the assembled Y chromosomes and performed a separate nanopolish run. Based on  
1134 the GRCh38 mappings we first performed sample quality control (QC). We find four samples with  
1135 genome wide methylation levels below 50%, which were QCed out. Using information on the multiple  
1136 runs on some samples we observed a high degree of concordance between multiple runs from the same  
1137 donor, average difference between the replicates over the segments of 0.01 [0-0.15] in methylation beta  
1138 space.

1139 After QC we leverage pycoMeth to *de novo* identify interesting methylation segments on  
1140 chromosome Y. pycoMeth (version 2.2)<sup>90</sup> Meth\_Seg is a Bayesian changepoint-detection algorithm  
1141 that determines regions with consistent methylation rate from the read-level methylation predictions.  
1142 Over the 139 QCed flowcells of the 41 samples, we find 2,861 segments that behave consistently in  
1143 terms of methylation variation in a sample. After segmentation we derived methylation rates per  
1144 segment per sample by binarizing methylation calls thresholded at absolute log-likelihood ratio of 2.

1145 To test for methylation effects of haplogroups we first leveraged the permanova test,  
1146 implemented in the R package vegan<sup>91,92</sup>, to identify the impact of “aggregated” haplotype group on  
1147 the DNAm levels over the segments. Because of the low sample numbers per haplotype group we  
1148 aggregated haplogroups to meta groups based on genomic distance and sample size. We aggregated

1149 A,B and C to “ABC”, G and H to “GH”, N and O to “NO”, and Q and R to “QR”. The E haplogroup  
1150 and J haplogroup were kept as individual units for our analyses. Additionally we tested for individual  
1151 segments with differential meta-haplogroup methylation differences using the Kruskal Wallis test.  
1152 Regions with  $FDR \leq 0.2$ , as derived from the Benjamini-Hochberg procedure, are reported as DMRs.  
1153 For follow up tests on the regions that are found to be significantly different from the Kruskal Wallis  
1154 test we used a one versus all strategy leveraging a Mann–Whitney U test.

1155 Next to assessing the effects of haplogroup to DNAm we also tested for local methylation  
1156 Quantitative Trait Loci (*cis*-meQTL) using limix-QTL<sup>93,94</sup>. Specifically, we tested the impact of the  
1157 genetic variants called on GRCh38 (see Methods “**Variant calling using *de novo* assemblies**”), versus  
1158 the DNAm levels in the 2,861 segments discovered by pycoMeth. For this we leveraged an LMM  
1159 implemented in limixQTL, methylation levels were arcsin transformed and we leveraged population as  
1160 a random effect term. Variants with a MAF >10% and a call rate >90%, leaving 11,226 variants to be  
1161 tested. For each DNAm segment we tested variants within the segment or within 100,000 bases around  
1162 it. Yielding a total of 245,131 tests. Using 1,000 permutations we determined the number of independent  
1163 tests per gene and P values were corrected for this estimated number of tests using the Bonferroni  
1164 procedure. To account for the number of tested segments we leveraged a Benjamini-Hochberg  
1165 procedure over the top variants per segment to correct for this.

1166

#### 1167 m. Expression analysis

1168 Gene expression quantification for the HGSVC<sup>11</sup> and the Geuvadis dataset<sup>26</sup> was derived from  
1169 the<sup>11</sup>. In short, RNA-seq QC was conducted using Trim Galore! (v0.6.5)<sup>95</sup> and reads were mapped to  
1170 GRCh38 using STAR (v2.7.5a)<sup>96</sup>, followed by gene expression quantification using FeatureCounts (v2)  
1171<sup>97</sup>. After quality control gene expression data is available for 210 Geuvadis males and 21 HGSVC males.

1172 As with the DNAm analysis we leveraged the permanova test to quantify the overall impact  
1173 of haplogroup on gene expression variation. Here we focused only on the Geuvadis samples initially  
1174 and tested for the effect of the signal character haplotype groups, specifically “E”, “G”, “I”, “J”, “N”, “R”  
1175 and “T”. Additionally we tested for single gene effects using the Kruskal Wallis test, and the Mann–  
1176 Whitney U test. For *BCORP1* we leveraged the HGSVC expression data to assess the link between  
1177 DNAm and expression variation.

1178

#### 1179 n. Iso-Seq data analysis

1180 Iso-Seq reads were aligned independently with minimap v2.24 (-ax splice:hq -f 1000) to each  
1181 chrY Verkko assembly, as well as the T2T v2.0 reference including HG002 chrY, and GRCh38. Read  
1182 alignments were compared between the HG002-T2T chrY reference and each *de novo* Verkko chrY  
1183 assembly. Existing testis Iso-seq data from seven individuals was also analyzed (SRX9033926 and  
1184 SRX9033927).

1185

1186 o. Hi-C data analysis

1187 We analyzed 40/43 samples for which Hi-C data was available (Hi-C data is missing for  
1188 HG00358, HG01890 and NA19705). For each sample, GRCh38 reference genome was used to map the  
1189 raw reads and Juicer software tools (version 1.6)<sup>98</sup> with the default aligner BWA mem (version: 0.7.17)  
1190<sup>99</sup> was utilized to preprocess and map the reads. Read pairs with low mapping quality (MAPQ < 30)  
1191 were filtered out and unmapped reads, such as abnormal split reads and duplicate reads, were also  
1192 removed. Using these filtered read pairs, Juicer was then applied to create a Hi-C contact map for each  
1193 sample. To leverage the collected chrY Hi-C data from these 40 samples with various resolutions, we  
1194 combined the chrY Hi-C contact maps of these 40 samples using the *mega.sh* script<sup>98</sup> given by Juicer  
1195 to produce a “mega” map. Knight-Ruiz (KR) matrix balancing was applied to normalize Hi-C contact  
1196 frequency matrices<sup>100</sup>.

1197 We then calculated Insulation Score (IS)<sup>101</sup>, which was initially developed to find TAD  
1198 boundaries on Hi-C data with a relatively low resolution, to call TAD boundaries at 10 kilobase  
1199 resolution for the merged sample and each individual sample. For the merged sample, the FAN-C toolkit  
1200 (version 0.9.23b4)<sup>102</sup> with default parameters was applied to calculate IS and boundary score (BS)  
1201 based on the KR normalized “mega” map at 10 kb resolution and 100 kb window size (utilizing the  
1202 same setting as in the 4DN domain calling protocol)<sup>103</sup>. For each individual sample, the KR normalized  
1203 contact matrix of each sample served as the input to the same procedure as in analyzing the merged  
1204 sample. The previous merged result was treated as a catalog of TAD boundaries in lymphoblastoid cell  
1205 lines (LCLs) for chrY to finalize the location of TAD boundaries and TADs of each individual sample.  
1206 More specifically, 25 kb flanking regions were added on both sides of the merged TAD boundary  
1207 locations. Any sample boundary located within the merged boundary with the added flanking region  
1208 was considered as the final TAD boundary. The final TAD regions were then derived from the two  
1209 adjacent TAD boundaries excluding those regions where more than half the length of the regions have  
1210 “NA” insulation score values.

1211 The average and variance (maximum difference between any of the two samples) insulation  
1212 scores of our 40 chrY samples were calculated to show the differences among these samples and were  
1213 plotted aligned with methylation analysis and chrY assembly together. Due to the limited Hi-C  
1214 sequencing depth and resolution, some of the chrY regions have the missing reads and those regions  
1215 with “NA” insulation scores were shown as blank regions in the plot. Kruskal-Wallis (One-Way  
1216 ANOVA) test (SciPy v1.7.3 `scipy.stats.kruskal`) was performed on the insulation scores (10 kb  
1217 resolution) of each sample with the same 6 meta haplogroups classified in the methylation analysis to  
1218 detect any associations between differentially insulated regions (DIR) and differentially methylated  
1219 regions (DMR). Within each DMR, P values were adjusted and those insulated regions with FDR ≤  
1220 0.20 were defined as the regions that are significantly differentially insulated and methylated.

1221

1222 p. Yq12 heterochromatin analyses

1223 Yq12 partitioning

1224 RepeatMasker (v4.1.0) was run using the default Dfam library to identify and classify repeat  
1225 elements within the sequence of the Yq12 region<sup>104</sup>. The RepeatMasker output was parsed to determine  
1226 the repeat organization and any recurring repeat patterns. A custom Python script that capitalized on the  
1227 patterns of repetitive elements, as well as the sequence length between *Alu* elements was used to identify  
1228 individual *DYZ2* repeats, as well as the start and end boundaries for each *DYZ1* and *DYZ2* array.

1229 Yq12 *DYZ2* consensus and divergence

1230 The two assemblies with the longest (T2T Y from HG002) and shortest (HG01890) Yq12  
1231 subregions were selected for *DYZ2* repeat consensus sequence building. Among all *DYZ2* repeats  
1232 identified within the Yq12 subregion, most (sample collective mean: 46.8%) were exactly 2,413 bp in  
1233 length. Therefore, five-hundred *DYZ2* repeats 2,413 bp in length were randomly selected from each  
1234 assembly, and their sequences retrieved using Pysam (version 0.19.1)<sup>105</sup>, ([https://github.com/pysam-](https://github.com/pysam-developers/pysam)  
1235 [developers/pysam](https://github.com/pysam-developers/pysam)). Next, a multiple sequence alignment (MSA) of these five-hundred sequences was  
1236 performed using Muscle (v5.1)<sup>106</sup>. Based on the MSA, a *DYZ2* consensus sequence was constructed  
1237 using a majority rule approach. Alignment of the two 2,413 bp consensus sequences, built from both  
1238 assemblies, confirmed 100% sequence identity between the two consensus sequences. Further analysis  
1239 of the *DYZ2* repeat regions revealed the absence of a seven nucleotide segment ('ACATACG') at the  
1240 intersection of the *DYZ2* HSATI and the adjacent *DYZ2* AT-rich simple repeat sequence. To address  
1241 this, ten nucleotides downstream of the HSAT I sequence of all *DYZ2* repeat units were retrieved, an  
1242 MSA performed using Muscle (v5.1)<sup>106</sup>, and a consensus sequence constructed using a majority rule  
1243 approach. The resulting consensus was then fused to the 2,413 bp consensus sequence creating a final  
1244 2,420 bp *DYZ2* consensus sequence. *DYZ2* arrays were then re-screened using HMMER (v3.3.2) and  
1245 the 2,420 bp *DYZ2* consensus sequence.

1246 In view of the AT-rich simple repeat portion of *DYZ2* being highly variable in length, only the  
1247 *Alu* and HSATI portion of the *DYZ2* consensus sequence was used as part of a custom RepeatMasker  
1248 library to determine the divergence of each *DYZ2* repeat sequence within the Yq12 subregion.  
1249 Divergence was defined as the percentage of substitutions in the sequence matching region compared  
1250 to the consensus. The *DYZ2* arrays were then visualized with a custom Turtle  
1251 (<https://docs.python.org/3.5/library/turtle.html#turtle.textinput>) script written in Python. To compare  
1252 the compositional similarity between *DYZ2* arrays within a genome, a *DYZ2* array (rows) by *DYZ2*  
1253 repeat composition profile (columns; *DYZ2* repeat length + orientation + divergence) matrix was  
1254 constructed. Next, the SciPy (v1.8.1) library was used to calculate the Bray-Curtis

1255 Distance/Dissimilarity (as implemented in `scipy.spatial.distance.braycurtis`) between *DYZ2* array  
1256 composition profiles<sup>107</sup>. The complement of the Bray-Curtis dissimilarity was used in the visualization  
1257 as typically a Bray-Curtis dissimilarity closer to zero implies that the two compositions are more similar  
1258 (**Fig. 4e, S49**).

#### 1259 Yq12 *DYZI* array analysis

1260 Initially, RepeatMasker (v4.1.0) was used to annotate all repeats within *DYZI* arrays. However,  
1261 consecutive RepeatMasker runs resulted in variable annotations. These variable results were also  
1262 observed using a custom RepeatMasker library approach with inclusion of the existing available *DYZI*  
1263 consensus sequence (Skaletsky et al 2003). In light of these findings, *DYZI* array sequences were  
1264 extracted with Pysam, and then each sequence underwent a virtual restriction digestion with HaeIII  
1265 using the Sequence Manipulation Suite<sup>108</sup>. HaeIII, which has a ‘ggcc’ restriction cut site, was chosen  
1266 based on previous research of the *DYZI* repeat in monozygotic twins<sup>109</sup>. The resulting restriction  
1267 fragment sequences were oriented based on the sequence orientation of satellite sequences within them  
1268 detected by RepeatMasker (base Dfam library). A new *DYZI* consensus sequence was constructed by  
1269 retrieving the sequence of digestion fragments 3,569 bp in length (as fragments this length were in the  
1270 greatest abundance in 6 out of 7 analyzed genomes), performing a MSA using Muscle (v5.1), and then  
1271 applying a majority rule approach to construct the consensus sequence.

1272 To classify the composition of all restriction fragments a k-mer profile analysis was performed.  
1273 First, the relative abundance of k-mers within fragments as well as consensus sequences (*DYZI8*, 3.1-  
1274 kbp, 2.7-kbp, *DYZI*) were computed. A k-mer of length 5 was chosen as *DYZI* is likely ancestrally  
1275 derived from a pentanucleotide<sup>4,110</sup>. Next, the Bray-Curtis dissimilarity between k-mer abundance  
1276 profiles of each fragment and consensus sequence was computed, and fragments were classified based  
1277 on their similarity to the consensus sequence k-mer profile (using a 75% similarity minimum) (**Fig.**  
1278 **S38**). Afterwards, the sequence fragments with the same classification adjacent to one another were  
1279 concatenated, and the fully assembled sequence was provided to HMMER (v3.3.2) to detect repeats and  
1280 partition fragment sequences into individual repeat units<sup>63</sup>. The HMMER output was filtered by E-  
1281 value (only E-value of zero was kept). Once individual repeat units (*DYZI8*, 3.1-kbp, 2.7-kbp, and  
1282 *DYZI*) were characterized (**Fig. S39**), the Bray-Curtis dissimilarity of their sequence k-mer profile  
1283 versus the consensus sequence was computed and then visualized with the custom Turtle script written  
1284 in Python (**Fig. S40**). A two-sided Mann-Whitney U test (SciPy v1.7.3 `scipy.stats.mannwhitneyu`<sup>107</sup>)  
1285 was utilized to test for differences in length between *DYZI* and *DYZ2* arrays for each sample with a  
1286 completely assembled Yq12 region (n=7) (T2T Y HG002:MWU=541.0, pvalue=0.000786;  
1287 HG02011:MWU=169.0, pvalue=0.000167; HG01106:MWU=617.0, pvalue=0.038162;  
1288 HG01952:MWU=172.0, pvalue=0.042480; HG01890:MWU=51.0, pvalue=0.000867;  
1289 HG02666:MWU=144.0, pvalue=0.007497; HG00358:MWU=497.0, pvalue=0.008068;) (**Fig. 4b**). A

1290 two-sided Spearman rank-order correlation coefficient (SciPy v1.7.3 `scipy.stats.spearmanr`<sup>107</sup>) was  
1291 calculated using all samples with a completely assembled Yq12 (n=7) to measure the relationship  
1292 between the total length of the analyzed Yq12 region and the total *DYZ1* plus *DYZ2* arrays within this  
1293 region (correlation=0.90093, p-value=0.005620) (**Fig. S46**). All statistical tests performed were  
1294 considered significant using an alpha=0.05.

## 1295 Yq12 Mobile Element Insertion Analysis

1296 RepeatMasker output was screened for the presence of additional transposable elements, in  
1297 particular mobile element insertions (MEIs). Putative MEIs (i.e., elements with a divergence <4%) plus  
1298 100 nt of flanking were retrieved from the respective assemblies. Following an MSA using Muscle, the  
1299 ancestral sequence of the MEI was determined and utilized for all downstream analyses, (This step was  
1300 necessary as some of the MEI duplicated multiple times and harbored substitutions). The divergence,  
1301 and subfamily affiliation, were determined based on the MEI with the lowest divergence from the  
1302 respective consensus sequence. All MEIs were screened for the presence of characteristics of target-  
1303 primed reverse transcription (TPRT) hallmarks (i.e., presence of an A-tail, target site duplications, and  
1304 endonuclease cleavage site)<sup>111</sup>.

## 1305 6. Statistical analysis and plotting

1306 All statistical analyses in this study were performed using R (<http://CRAN.R-project.org/>) and  
1307 Python (<http://www.python.org>). The respective test details such as program or library version, sample  
1308 size, resulting statistics and p-values are stated in the running text. Figures were generated using R and  
1309 Python's Matplotlib (<https://matplotlib.org>), seaborn<sup>68</sup> and the "Turtle" graphics framework  
1310 (<https://docs.python.org/3/library/turtle.html>).

## 1311 7. Data Availability

1312 All data generated are available via the HGSVC data portal at  
1313 [https://ftp.1000genomes.ebi.ac.uk/vol1/ftp/data\\_collections/HGSVC2/working/](https://ftp.1000genomes.ebi.ac.uk/vol1/ftp/data_collections/HGSVC2/working/) and  
1314 [https://ftp.1000genomes.ebi.ac.uk/vol1/ftp/data\\_collections/HGSVC3/working/](https://ftp.1000genomes.ebi.ac.uk/vol1/ftp/data_collections/HGSVC3/working/). HPRC year 1 data  
1315 files, PacBio HiFi, Oxford Nanopore (ONT) long-read sequencing and Bionano Genomics optical  
1316 mapping and data files were downloaded from the following url: <https://humanpangenome.org/year-1-sequencing-data-release/>.  
1317



## 1318 8. Code Availability

1319 Project code implemented to produce the assemblies and the basic QC/evaluation statistics is  
1320 available at [github.com/marschall-lab/project-male-assembly](https://github.com/marschall-lab/project-male-assembly). All scripts written and used in the study  
1321 of the Yq12 subregion are available at <https://github.com/Markloftus/Yq12>.

## 1322 Author contributions

1323 PacBio production sequencing: Q.Z., K.M.M., A.P.L., J.K.; ONT production: Q.Z., K.H.;  
1324 Strand-seq production: P.Hasenfeld, J.O.K.; ONT re-basecalling and methylation calling: P.A.A.,  
1325 W.T.H.; Genome assembly: P.E., F.Y., T.M.; Assembly analysis and evaluation: P.E., P.H., F.Y., W.H.,  
1326 F.T.; Assembly-based variant calling: P.E., P.A.A., P.H., C.R.B.; Variant QC, merging, and annotation:  
1327 P.A.A., P.H.; Short-read calling, phylogeny construction and dating: P.H.; Analysis of Bionano  
1328 Genomics optical maps: F.Y.; Strand-seq inversion detection and genotyping: D.P.; MEI discovery and  
1329 integration: W.Z., M.L., M.K.K.; Inversion analysis: P.H., D.P., K.K., M.L., M.K.K.; Analyses on Y  
1330 subregions: P.E., P.H., M.L., F.Y., G.A.L., P.A.A., W.H., K.K., F.T., M.K.K., E.E.E., C.L.; RNA-seq  
1331 analysis: M.J.B.; Methylation and meQTL analysis: M.J.B.; HiC analysis: C.Li., X.S.; Iso-Seq analysis:  
1332 P.D., E.E.E.; Gene annotations F.Y., P.D.; Supplementary materials: P.H., P.E., M.L., F.Y., P.A.A.,  
1333 G.A.L., M.J.B., W.Z., W.H., K.K., C.Li, P.D., F.T., J.Y.K., Q.Z., K.M.M., P.Hasenfeld, X.S., M.K.K.;  
1334 Display items: P.H., P.E., M.L., F.Y., G.A.L., W.H., K.K., F.T., M.K.K.; Manuscript writing: P.H.,  
1335 P.E., M.L., P.A.A, G.A.L., M.J.B., W.Z., M.K.K., C.L. with contributions from all other authors. All  
1336 authors contributed to the final interpretation of data. HGSVC Co-chairs: C.L., J.O.K., E.E.E., T.M.

## 1337 Acknowledgements

1338 We thank Dr. Yali Xue for discussions and advice throughout the project; Jonathan Wood and  
1339 the Genome Reference Informatics Team at the Wellcome Sanger Institute for suggestions and feedback  
1340 on assembly evaluation; the Human Pangenome Reference Consortium (HPRC,  
1341 <https://humanpangenome.org>) for making their data publicly available; the Centre for Information and  
1342 Media Technology at Heinrich Heine University Düsseldorf and the Scientific Services at the Jackson  
1343 Laboratory including the Genome Technologies Service for their expert assistance with the work  
1344 described herein and Research IT for providing computational infrastructure and support and the  
1345 Phillippy Lab (NIH/NHGRI) for their comprehensive Verkko support. We are grateful to the people  
1346 who generously contributed samples as part of the 1000 Genomes Project.

## 1347 Funding

1348 Funding was provided by National Institutes of Health (NIH) grants U24HG007497 (to C.L.,  
1349 E.E.E., J.O.K., T.M.), U01HG010973 (to T.M., E.E.E., and J.O.K.), and R01HG002385 and  
1350 R01HG010169 (to E.E.E.); the German Federal Ministry for Research and Education (BMBF  
1351 031L0184 to J.O.K. and T.M.); the German Research Foundation (DFG 391137747 to T.M.); the  
1352 German Human Genome-Phenome Archive (DFG [NFDI 1/1] to J.O.K.); the European Research  
1353 Council (ERC Consolidator grant 773026 to J.O.K.); the EMBL (J.O.K. and P.Hasenfeld); the EMBL  
1354 International PhD Programme (W.H.); the Jackson Laboratory Postdoctoral Scholar Award (K.K.); NIH  
1355 National Institute of General Medical Sciences (NIGMS R35GM133600 to C.R.B.; 1P20GM139769 to  
1356 M.K.K. and M.L.) and National Cancer Institute (NCI) (P30CA034196 to C.R.B. and P.A.A.);  
1357 U24HG007497 (P. H., F.Y., Q.Z., F.T., J.Y.K.); NIGMS K99GM147352 (G.A.L.) and Wellcome grant  
1358 098051 (to C.T.-S.). E.E.E. is an investigator of the Howard Hughes Medical Institute.

## 1359 Competing interests

1360 E.E.E. is a scientific advisory board (SAB) member of Variant Bio. C.L. is an SAB member of  
1361 Nabsys and Genome Insight. The following authors have previously disclosed a patent application (no.  
1362 EP19169090) relevant to Strand-seq: J.O.K., T.M., and D.P.; the other authors declare no competing  
1363 interests.

1364

## 1365 References

- 1366 1. Charlesworth, B. & Charlesworth, D. The degeneration of Y chromosomes. *Philos. Trans. R.*  
1367 *Soc. Lond. B Biol. Sci.* **355**, 1563–1572 (2000).
- 1368 2. Vollger, M. R. *et al.* Segmental duplications and their variation in a complete human genome.  
1369 *Science* **376**, eabj6965 (2022).
- 1370 3. Skaletsky, H. *et al.* The male-specific region of the human Y chromosome is a mosaic of discrete  
1371 sequence classes. *Nature* **423**, 825–837 (2003).
- 1372 4. Altemose, N., Miga, K. H., Maggioni, M. & Willard, H. F. Genomic characterization of large  
1373 heterochromatic gaps in the human genome assembly. *PLoS Comput. Biol.* **10**, e1003628 (2014).
- 1374 5. Nakahori, Y., Mitani, K., Yamada, M. & Nakagome, Y. A human Y-chromosome specific  
1375 repeated DNA family (DYZ1) consists of a tandem array of pentanucleotides. *Nucleic Acids*  
1376 *Research* vol. 14 7569–7580 Preprint at <https://doi.org/10.1093/nar/14.19.7569> (1986).
- 1377 6. Cooke, H. Repeated sequence specific to human males. *Nature* **262**, 182–186 (1976).
- 1378 7. Skov, L., Danish Pan Genome Consortium & Schierup, M. H. Analysis of 62 hybrid assembled  
1379 human Y chromosomes exposes rapid structural changes and high rates of gene conversion.  
1380 *PLoS Genet.* **13**, e1006834 (2017).
- 1381 8. Kuderna, L. F. K. *et al.* Selective single molecule sequencing and assembly of a human Y  
1382 chromosome of African origin. *Nat. Commun.* **10**, 4 (2019).
- 1383 9. Sahakyan, H. *et al.* Origin and diffusion of human Y chromosome haplogroup J1-M267. *Sci.*  
1384 *Rep.* **11**, 6659 (2021).
- 1385 10. Rhie, A. *et al.* The complete sequence of a human Y chromosome. bioRxiv 2022.
- 1386 11. Ebert, P. *et al.* Haplotype-resolved diverse human genomes and integrated analysis of structural  
1387 variation. *Science* **372**, (2021).
- 1388 12. Liao, W.-W. *et al.* A Draft Human Pangenome Reference. *bioRxiv* 2022.07.09.499321 (2022)  
1389 doi:10.1101/2022.07.09.499321.
- 1390 13. Poznik, G. D. *et al.* Punctuated bursts in human male demography inferred from 1,244  
1391 worldwide Y-chromosome sequences. *Nat. Genet.* **48**, 593–599 (2016).
- 1392 14. Karmin, M. *et al.* A recent bottleneck of Y chromosome diversity coincides with a global change  
1393 in culture. *Genome Res.* **25**, 459–466 (2015).
- 1394 15. Hallast, P., Agdzhoyan, A., Balanovsky, O., Xue, Y. & Tyler-Smith, C. A Southeast Asian origin  
1395 for present-day non-African human Y chromosomes. *Hum. Genet.* **140**, 299–307 (2021).
- 1396 16. Y Chromosome Consortium. A nomenclature system for the tree of human Y-chromosomal  
1397 binary haplogroups. *Genome Res.* **12**, 339–348 (2002).
- 1398 17. Mendez, F. L. *et al.* An African American paternal lineage adds an extremely ancient root to the  
1399 human Y chromosome phylogenetic tree. *Am. J. Hum. Genet.* **92**, 454–459 (2013).
- 1400 18. Rautiainen, M. *et al.* Verkko: telomere-to-telomere assembly of diploid chromosomes. *bioRxiv*

- 1401 2022.06.24.497523 (2022) doi:10.1101/2022.06.24.497523.
- 1402 19. Mikheenko, A., Bzikadze, A. V., Gurevich, A., Miga, K. H. & Pevzner, P. A. TandemTools:  
1403 mapping long reads and assessing/improving assembly quality in extra-long tandem repeats.  
1404 *Bioinformatics* **36**, i75–i83 (2020).
- 1405 20. Yan, Y. *et al.* Copy number variation of functional RBMY1 is associated with sperm motility: an  
1406 azoospermia factor-linked candidate for asthenozoospermia. *Hum. Reprod.* **32**, 1521–1531  
1407 (2017).
- 1408 21. Gegenschatz-Schmid, K., Verkauskas, G., Stadler, M. B. & Hadziselimovic, F. Genes located in  
1409 Y-chromosomal regions important for male fertility show altered transcript levels in  
1410 cryptorchidism and respond to curative hormone treatment. *Basic Clin Androl* **29**, 8 (2019).
- 1411 22. Porubsky, D. *et al.* Recurrent inversion polymorphisms in humans associate with genetic  
1412 instability and genomic disorders. *Cell* **185**, 1986–2005.e26 (2022).
- 1413 23. Hammer, M. F. A recent insertion of an alu element on the Y chromosome is a useful marker for  
1414 human population studies. *Mol. Biol. Evol.* **11**, 749–761 (1994).
- 1415 24. Babcock, M., Yatsenko, S., Stankiewicz, P., Lupski, J. R. & Morrow, B. E. AT-rich repeats  
1416 associated with chromosome 22q11.2 rearrangement disorders shape human genome architecture  
1417 on Yq12. *Genome Res.* **17**, 451–460 (2007).
- 1418 25. Smith, G. P. Evolution of repeated DNA sequences by unequal crossover. *Science* **191**, 528–535  
1419 (1976).
- 1420 26. Lappalainen, T. *et al.* Transcriptome and genome sequencing uncovers functional variation in  
1421 humans. *Nature* **501**, 506–511 (2013).
- 1422 27. Miga, K. H. *et al.* Centromere reference models for human chromosomes X and Y satellite  
1423 arrays. *Genome Res.* **24**, 697–707 (2014).
- 1424 28. Oakey, R. & Tyler-Smith, C. Y chromosome DNA haplotyping suggests that most European and  
1425 Asian men are descended from one of two males. *Genomics* **7**, 325–330 (1990).
- 1426 29. Miga, K. H. *et al.* Telomere-to-telomere assembly of a complete human X chromosome. *Nature*  
1427 **585**, 79–84 (2020).
- 1428 30. Logsdon, G. A. *et al.* The structure, function and evolution of a complete human chromosome 8.  
1429 *Nature* **593**, 101–107 (2021).
- 1430 31. Altemose, N. *et al.* Complete genomic and epigenetic maps of human centromeres. *Science* **376**,  
1431 eabl4178 (2022).
- 1432 32. Gershman, A. *et al.* Epigenetic patterns in a complete human genome. *Science* **376**, eabj5089  
1433 (2022).
- 1434 33. Cooke, H. J. & McKay, R. D. Evolution of a human Y chromosome-specific repeated sequence.  
1435 *Cell* **13**, 453–460 (1978).
- 1436 34. Rahman, M. M., Bashamboo, A., Prasad, A., Pathak, D. & Ali, S. Organizational variation of  
1437 DYZ1 repeat sequences on the human Y chromosome and its diagnostic potentials. *DNA Cell*

- 1438 *Biol.* **23**, 561–571 (2004).
- 1439 35. Pathak, D., Premi, S., Srivastava, J., Chandy, S. P. & Ali, S. Genomic instability of the DYZ1  
1440 repeat in patients with Y chromosome anomalies and males exposed to natural background  
1441 radiation. *DNA Res.* **13**, 103–109 (2006).
- 1442 36. Manz, E., Alkan, M., Bühler, E. & Schmidtke, J. Arrangement of DYZ1 and DYZ2 repeats on  
1443 the human Y-chromosome: a case with presence of DYZ1 and absence of DYZ2. *Mol. Cell.*  
1444 *Probes* **6**, 257–259 (1992).
- 1445 37. Lange, J. *et al.* Isodicentric Y chromosomes and sex disorders as byproducts of homologous  
1446 recombination that maintains palindromes. *Cell* **138**, 855–869 (2009).
- 1447 38. Sturtevant, A. H. Genetic Factors Affecting the Strength of Linkage in *Drosophila*. *Proc. Natl.*  
1448 *Acad. Sci. U. S. A.* **3**, 555–558 (1917).
- 1449 39. Verma, R. S. *Heterochromatin: Molecular and Structural Aspects*. (Cambridge University Press,  
1450 1988).
- 1451 40. Tyler-Smith, C. & Brown, W. R. Structure of the major block of alphoid satellite DNA on the  
1452 human Y chromosome. *J. Mol. Biol.* **195**, 457–470 (1987).
- 1453 41. Cooper, K. F., Fisher, R. B. & Tyler-Smith, C. Structure of the sequences adjacent to the  
1454 centromeric alphoid satellite DNA array on the human Y chromosome. *J. Mol. Biol.* **230**, 787–  
1455 799 (1993).
- 1456 42. 1000 Genomes Project Consortium *et al.* A global reference for human genetic variation. *Nature*  
1457 **526**, 68–74 (2015).
- 1458 43. Logsdon, G. HMW gDNA purification and ONT ultra-long-read data generation v3. (2022)  
1459 doi:10.17504/protocols.io.b55tq86n.
- 1460 44. Gong, L., Wong, C.-H., Idol, J., Ngan, C. Y. & Wei, C.-L. Ultra-long Read Sequencing for  
1461 Whole Genomic DNA Analysis. *J. Vis. Exp.* (2019) doi:10.3791/58954.
- 1462 45. Sanders, A. D., Falconer, E., Hills, M., Spierings, D. C. J. & Lansdorp, P. M. Single-cell  
1463 template strand sequencing by Strand-seq enables the characterization of individual homologs.  
1464 *Nat. Protoc.* **12**, 1151–1176 (2017).
- 1465 46. Falconer, E. *et al.* DNA template strand sequencing of single-cells maps genomic rearrangements  
1466 at high resolution. *Nat. Methods* **9**, 1107–1112 (2012).
- 1467 47. Sanders, A. D. *et al.* Single-cell analysis of structural variations and complex rearrangements  
1468 with tri-channel processing. *Nat. Biotechnol.* **38**, 343–354 (2020).
- 1469 48. Byrska-Bishop, M. *et al.* High-coverage whole-genome sequencing of the expanded 1000  
1470 Genomes Project cohort including 602 trios. *Cell* **185**, 3426–3440.e19 (2022).
- 1471 49. Poznik, G. D. *et al.* Sequencing Y chromosomes resolves discrepancy in time to common  
1472 ancestor of males versus females. *Science* **341**, 562–565 (2013).
- 1473 50. Danecek, P. *et al.* Twelve years of SAMtools and BCFtools. *Gigascience* **10**, (2021).
- 1474 51. Li, H. A statistical framework for SNP calling, mutation discovery, association mapping and

- 1475 population genetical parameter estimation from sequencing data. *Bioinformatics* **27**, 2987–2993  
1476 (2011).
- 1477 52. Danecek, P. *et al.* The variant call format and VCFtools. *Bioinformatics* **27**, 2156–2158 (2011).
- 1478 53. Drummond, A. J. & Rambaut, A. BEAST: Bayesian evolutionary analysis by sampling trees.  
1479 *BMC Evol. Biol.* **7**, 214 (2007).
- 1480 54. Stamatakis, A. RAxML version 8: a tool for phylogenetic analysis and post-analysis of large  
1481 phylogenies. *Bioinformatics* **30**, 1312–1313 (2014).
- 1482 55. Fu, Q. *et al.* Genome sequence of a 45,000-year-old modern human from western Siberia. *Nature*  
1483 **514**, 445–449 (2014).
- 1484 56. Mölder, F. *et al.* Sustainable data analysis with Snakemake. *F1000Res.* **10**, 33 (2021).
- 1485 57. Cheng, H., Concepcion, G. T., Feng, X., Zhang, H. & Li, H. Haplotype-resolved de novo  
1486 assembly using phased assembly graphs with hifiasm. *Nat. Methods* **18**, 170–175 (2021).
- 1487 58. Li, H. Minimap2: pairwise alignment for nucleotide sequences. *Bioinformatics* **34**, 3094–3100  
1488 (2018).
- 1489 59. Mistry, J., Finn, R. D., Eddy, S. R., Bateman, A. & Punta, M. Challenges in homology search:  
1490 HMMER3 and convergent evolution of coiled-coil regions. *Nucleic Acids Res.* **41**, e121 (2013).
- 1491 60. Poplin, R. *et al.* A universal SNP and small-indel variant caller using deep neural networks. *Nat.*  
1492 *Biotechnol.* **36**, 983–987 (2018).
- 1493 61. Shafin, K. *et al.* Haplotype-aware variant calling with PEPPER-Margin-DeepVariant enables  
1494 high accuracy in nanopore long-reads. *Nat. Methods* **18**, 1322–1332 (2021).
- 1495 62. Teitz, L. S., Pyntikova, T., Skaletsky, H. & Page, D. C. Selection Has Countered High Mutability  
1496 to Preserve the Ancestral Copy Number of Y Chromosome Amplicons in Diverse Human  
1497 Lineages. *Am. J. Hum. Genet.* **103**, 261–275 (2018).
- 1498 63. Eddy, S. R. Accelerated Profile HMM Searches. *PLoS Comput. Biol.* **7**, e1002195 (2011).
- 1499 64. Shepelev, V. A. *et al.* Annotation of suprachromosomal families reveals uncommon types of  
1500 alpha satellite organization in pericentromeric regions of hg38 human genome assembly. *Genom*  
1501 *Data* **5**, 139–146 (2015).
- 1502 65. Altomose, N. A classical revival: Human satellite DNAs enter the genomics era. *Semin. Cell*  
1503 *Dev. Biol.* **128**, 2–14 (2022).
- 1504 66. Pedersen, B. S. & Quinlan, A. R. Mosdepth: quick coverage calculation for genomes and  
1505 exomes. *Bioinformatics* **34**, 867–868 (2018).
- 1506 67. Quinlan, A. R. & Hall, I. M. BEDTools: a flexible suite of utilities for comparing genomic  
1507 features. *Bioinformatics* **26**, 841–842 (2010).
- 1508 68. Waskom, M. seaborn: statistical data visualization. *J. Open Source Softw.* **6**, 3021 (2021).
- 1509 69. Hunter, J. D. Matplotlib: A 2D Graphics Environment. *Comput. Sci. Eng.* **9**, 90–95 (2007).
- 1510 70. Seabold, S. & Perktold, J. Statsmodels: Econometric and statistical modeling with python. in  
1511 *Proceedings of the 9th Python in Science Conference (SciPy, 2010)*. doi:10.25080/majora-

- 1512 92bf1922-011.
- 1513 71. Altschul, S. F., Gish, W., Miller, W., Myers, E. W. & Lipman, D. J. Basic local alignment search  
1514 tool. *J. Mol. Biol.* **215**, 403–410 (1990).
- 1515 72. Guy, L., Kultima, J. R. & Andersson, S. G. E. genoPlotR: comparative gene and genome  
1516 visualization in R. *Bioinformatics* **26**, 2334–2335 (2010).
- 1517 73. Vollger, M. R., Kerpedjiev, P., Phillippy, A. M. & Eichler, E. E. StainedGlass: Interactive  
1518 visualization of massive tandem repeat structures with identity heatmaps. *Bioinformatics* (2022)  
1519 doi:10.1093/bioinformatics/btac018.
- 1520 74. Fenner, J. N. Cross-cultural estimation of the human generation interval for use in genetics-based  
1521 population divergence studies. *Am. J. Phys. Anthropol.* **128**, 415–423 (2005).
- 1522 75. Katoh, K. & Standley, D. M. MAFFT multiple sequence alignment software version 7:  
1523 improvements in performance and usability. *Mol. Biol. Evol.* **30**, 772–780 (2013).
- 1524 76. Katoh, K., Misawa, K., Kuma, K.-I. & Miyata, T. MAFFT: a novel method for rapid multiple  
1525 sequence alignment based on fast Fourier transform. *Nucleic Acids Res.* **30**, 3059–3066 (2002).
- 1526 77. Benson, G. Tandem repeats finder: a program to analyze DNA sequences. *Nucleic Acids Res.* **27**,  
1527 573–580 (1999).
- 1528 78. Castresana, J. Selection of conserved blocks from multiple alignments for their use in  
1529 phylogenetic analysis. *Mol. Biol. Evol.* **17**, 540–552 (2000).
- 1530 79. Ren, J. & Chaisson, M. J. P. Ira: A long read aligner for sequences and contigs. *PLoS Comput.*  
1531 *Biol.* **17**, e1009078 (2021).
- 1532 80. Heller, D. & Vingron, M. SVIM-asm: Structural variant detection from haploid and diploid  
1533 genome assemblies. *Bioinformatics* (2020) doi:10.1093/bioinformatics/btaa1034.
- 1534 81. Smolka, M. *et al.* Comprehensive Structural Variant Detection: From Mosaic to Population-  
1535 Level. *bioRxiv* 2022.04.04.487055 (2022) doi:10.1101/2022.04.04.487055.
- 1536 82. Wenger, A. M. *et al.* Accurate circular consensus long-read sequencing improves variant  
1537 detection and assembly of a human genome. *Nat. Biotechnol.* **37**, 1155–1162 (2019).
- 1538 83. Zheng, Z. *et al.* Symphonizing pileup and full-alignment for deep learning-based long-read  
1539 variant calling. *bioRxiv* 2021.12.29.474431 (2021) doi:10.1101/2021.12.29.474431.
- 1540 84. Jiang, T. *et al.* Long-read-based human genomic structural variation detection with cuteSV.  
1541 *Genome Biol.* **21**, 189 (2020).
- 1542 85. Edge, P. & Bansal, V. Longshot enables accurate variant calling in diploid genomes from single-  
1543 molecule long read sequencing. *Nat. Commun.* **10**, 4660 (2019).
- 1544 86. Audano, P. A. *et al.* Characterizing the Major Structural Variant Alleles of the Human Genome.  
1545 *Cell* **176**, 663–675.e19 (2019).
- 1546 87. Xue, Y. & Tyler-Smith, C. An Exceptional Gene: Evolution of the TSPY Gene Family in  
1547 Humans and Other Great Apes. *Genes* **2**, 36–47 (2011).
- 1548 88. Zhou, W. *et al.* Identification and characterization of occult human-specific LINE-1 insertions

- 1549 using long-read sequencing technology. *Nucleic Acids Res.* **48**, 1146–1163 (2020).
- 1550 89. Shumate, A. & Salzberg, S. L. Liftoff: accurate mapping of gene annotations. *Bioinformatics*  
1551 (2020) doi:10.1093/bioinformatics/btaa1016.
- 1552 90. Snajder, R., Leger, A., Stegle, O. & Bonder, M. J. pycoMeth: A toolbox for differential  
1553 methylation testing from Nanopore methylation calls. *bioRxiv* 2022.02.16.480699 (2022)  
1554 doi:10.1101/2022.02.16.480699.
- 1555 91. The R Project for Statistical Computing. <https://www.R-project.org/>.
- 1556 92. Community Ecology Package [R package vegan version 2.6-4]. (2022).
- 1557 93. Cuomo, A. S. E. *et al.* Optimizing expression quantitative trait locus mapping workflows for  
1558 single-cell studies. *Genome Biol.* **22**, 188 (2021).
- 1559 94. Casale, F. P., Rakitsch, B., Lippert, C. & Stegle, O. Efficient set tests for the genetic analysis of  
1560 correlated traits. *Nat. Methods* **12**, 755–758 (2015).
- 1561 95. Krueger. Trim Galore: a wrapper tool around Cutadapt and FastQC to consistently apply quality  
1562 and adapter trimming to FastQ files, with some extra functionality for .... URL [http://www.](http://www.bioinformatics.babraham.ac.uk)  
1563 *bioinformatics.babraham.ac.uk*.
- 1564 96. Dobin, A. *et al.* STAR: ultrafast universal RNA-seq aligner. *Bioinformatics* **29**, 15–21 (2013).
- 1565 97. Liao, Y., Smyth, G. K. & Shi, W. The Subread aligner: fast, accurate and scalable read mapping  
1566 by seed-and-vote. *Nucleic Acids Res.* **41**, e108 (2013).
- 1567 98. Durand, N. C. *et al.* Juicer Provides a One-Click System for Analyzing Loop-Resolution Hi-C  
1568 Experiments. *Cell Syst* **3**, 95–98 (2016).
- 1569 99. Li, H. & Durbin, R. Fast and accurate long-read alignment with Burrows-Wheeler transform.  
1570 *Bioinformatics* **26**, 589–595 (2010).
- 1571 100. Knight, P. A. & Ruiz, D. A fast algorithm for matrix balancing. *IMA J. Numer. Anal.* **33**, 1029–  
1572 1047 (2012).
- 1573 101. Crane, E. *et al.* Condensin-driven remodelling of X chromosome topology during dosage  
1574 compensation. *Nature* **523**, 240–244 (2015).
- 1575 102. Kruse, K., Hug, C. B. & Vaquerizas, J. M. FAN-C: a feature-rich framework for the analysis and  
1576 visualisation of chromosome conformation capture data. *Genome Biol.* **21**, 303 (2020).
- 1577 103. Dekker, J. *et al.* The 4D nucleome project. *Nature* **549**, 219–226 (2017).
- 1578 104. Storer, J., Hubley, R., Rosen, J., Wheeler, T. J. & Smit, A. F. The Dfam community resource of  
1579 transposable element families, sequence models, and genome annotations. *Mob. DNA* **12**, 2  
1580 (2021).
- 1581 105. Li, H. *et al.* The Sequence Alignment/Map format and SAMtools. *Bioinformatics* **25**, 2078–2079  
1582 (2009).
- 1583 106. Edgar, R. C. MUSCLE: multiple sequence alignment with high accuracy and high throughput.  
1584 *Nucleic Acids Res.* **32**, 1792–1797 (2004).
- 1585 107. Virtanen, P. *et al.* SciPy 1.0: fundamental algorithms for scientific computing in Python. *Nat.*



- 1586            *Methods* **17**, 261–272 (2020).
- 1587    108. Stothard, P. The sequence manipulation suite: JavaScript programs for analyzing and formatting  
1588            protein and DNA sequences. *Biotechniques* **28**, 1102, 1104 (2000).
- 1589    109. Yadav, S. K., Kumari, A., Javed, S. & Ali, S. DYZ1 arrays show sequence variation between the  
1590            monozygotic males. *BMC Genet.* **15**, 19 (2014).
- 1591    110. Prosser, J., Frommer, M., Paul, C. & Vincent, P. C. Sequence relationships of three human  
1592            satellite DNAs. *J. Mol. Biol.* **187**, 145–155 (1986).
- 1593    111. Konkel, M. K., Walker, J. A. & Batzer, M. A. LINEs and SINEs of primate evolution. *Evol.*  
1594            *Anthropol.* **19**, 236–249 (2010).

1595